

IGF2BP1 enhances an aggressive tumor cell phenotype by impairing miRNA-directed downregulation of oncogenic factors

Simon Müller[†], Nadine Bley[†], Markus Glaß[†], Bianca Busch, Vanessa Rousseau, Danny Misiak, Tommy Fuchs, Marcell Lederer and Stefan Hüttelmaier*

Institute of Molecular Medicine, Section for Molecular Cell Biology, Faculty of Medicine, Martin Luther University Halle-Wittenberg, Kurt-Mothes-Str. 3a, 06120 Halle, Germany

Received August 10, 2017; Revised March 06, 2018; Editorial Decision March 14, 2018; Accepted March 20, 2018

ABSTRACT

The oncofetal IGF2 mRNA binding proteins (IGF2BPs) are upregulated in most cancers but their paralogue-specific roles in tumor cells remain poorly understood. In a panel of five cancer-derived cell lines, IGF2BP1 shows highly conserved oncogenic potential. Consistently, the deletion of IGF2BP1 impairs the growth and metastasis of ovarian cancer-derived cells in nude mice. Gene expression analyses in ovarian cancer-derived cells reveal that the knockdown of IGF2BPs is associated with the downregulation of mRNAs that are prone to miRNA regulation. All three IGF2BPs preferentially associate upstream of miRNA binding sites (MBSs) in the 3'UTR of mRNAs. The downregulation of mRNAs co-regulated by miRNAs and IGF2BP1 is abrogated at low miRNA abundance or when miRNAs are depleted. IGF2BP1 associates with these target mRNAs in RISC-free complexes and its deletion enhances their association with AGO2. The knockdown of most miRNA-regulated target mRNAs of IGF2BP1 impairs tumor cell properties. In four primary cancers, elevated synthesis of these target mRNAs is largely associated with upregulated IGF2BP1 mRNA levels. In ovarian cancer, the enhanced expression of IGF2BP1 and most of its miRNA-controlled target mRNAs is associated with poor prognosis. In conclusion, these findings indicate that IGF2BP1 enhances an aggressive tumor cell phenotype by antagonizing miRNA-impaired gene expression.

INTRODUCTION

MicroRNAs (miRNAs, miRs) are highly conserved and abundant small non-coding RNAs inhibiting gene expression by inducing target mRNA degradation and/or the inhibition of translation (1). They influence virtually all cell functions and play vital roles in controlling development and differentiation. Deregulated miRNA expression and/or function has been reported in essentially all human diseases including cancer where miRNAs serve oncogenic as well as tumor suppressive roles (2,3). One prominent example is the let-7 miRNA family. This miRNA family is highly conserved and acts in a tumor suppressive manner by interfering with the synthesis of oncogenic factors including H/KRAS, MYC/N, HMGA2 and LIN28A/B to name a few (4–8). However, although downregulated in most cancers including ovarian carcinomas (9), let-7 miRNAs still sum up to one of the most abundant miRNA families in most cancer-derived cells. This strongly suggests mechanisms impairing miRNA action in cancer. One obvious way of escaping miRNA-directed regulation is the 'deletion' of miRNA binding sites (MBSs) by shortening 3'UTRs via alternative polyadenylation. This has been reported for upregulated HMGA2 and IGF2BP1 expression in aggressive cancers (10,11). However, the longest and thus 'miRNA-prone' 3'UTRs of mRNAs like IGF2BP1 are maintained in some aggressive cancers (12). Alternatively, miRNAs may be 'sponged' and thus sequestered by the upregulated expression of mRNAs comprising MBSs for tumor-suppressive miRNAs. This was proposed for neuroblastoma where the amplification of the MYCN gene was suggested to impair let-7 activity (13). However, how the miRNA-sequestering transcripts escape miRNA-directed degradation allowing the sustained synthesis of oncogenic factors like HMGA2 or MYCs remains controversial. Finally, some RNA-binding proteins (RBPs) have been reported to either promote or impair the miRNA-directed degradation of target mRNAs (14).

*To whom correspondence should be addressed. Tel: +49 345 5573959; Fax: +49 345 557126; Email: stefan.huettelmaier@medizin.uni-halle.de

[†]The authors wish it to be known that, in their opinion, the first three authors should be regarded as Joint First Authors.

The oncofetal IGF2 mRNA binding proteins (IGF2BPs; alias: VICKZ, CRD-BP, IMPs or ZBPs) present an oncogenic family of RBPs reported to control mRNA transport, translation and turnover during development and in cancer cells (15). IGF2BP1 and 3 are *bona fide* oncofetal proteins with high expression during embryogenesis and *de novo* synthesis or significant upregulation in various tumors (15,16). IGF2BP2 is the only family member with ubiquitous expression in the adult organism (15). All three IGF2BPs were shown to promote an ‘aggressive’ tumor cell phenotype. IGF2BP1 and 3 enhance the viability, growth, migration, invasion and/or metastatic potential of tumor-derived cells *in vitro* and *in vivo* (17–22). Both these IGF2BPs are frequently co-upregulated in cancer suggesting shared upstream effectors, presumably including the oncogene MYC, promoting their expression (23). Elevated expression of IGF2BPs has also been reported in progenitor cells and all three IGF2BPs were suggested to sustain stem-cell properties in non-transformed as well as cancer cells (24–26).

Recent reports indicate that the loss of DICER induces a partially irreversible epigenetic shift inducing a pan-cancer gene expression signature including all three IGF2BPs (27). In the respective study, the loss of all three IGF2BPs substantially interfered with the ‘oncogenic potential’ of DICER-deleted and re-expressing cells. This suggests that IGF2BPs are key modulators of miRNA-controlled gene expression in cancer. Consistently, IGF2BP1 antagonizes the tumor suppressive action of the let-7 family in ovarian cancer-derived cells via a self-sustaining oncogenic triangle comprising IGF2BP1, HMGA2 and LIN28B (12). IGF2BP2 was proposed to support glioblastoma stem cell maintenance by impairing the inhibition of gene expression by let-7 miRNAs, and IGF2BP3 was shown to interfere with the downregulation of HMGA2 by let-7 miRNAs (24,28). These studies suggested that all three IGF2BPs promote tumorigenesis by interfering with the miRNA-directed degradation of oncogene-encoding mRNAs in cancer cells.

Starting from ovarian cancer in which elevated expression of all three IGF2BPs was reported to promote tumorigenesis (17,29,30), we analyzed the phenotypic roles of IGF2BPs in five tumor cell lines derived from distinct solid cancers. These studies revealed that IGF2BP1 has the most conserved ‘oncogenic potential’ of all three IGF2BPs. The protein enhances an ‘aggressive’ tumor cell phenotype largely by impairing the miRNA-directed downregulation of mRNAs.

MATERIALS AND METHODS

Plasmids and cloning

Cloning strategies including vectors, oligonucleotides used for PCR and restriction sites are summarized in Supplementary Table T5. All constructs were validated by sequencing.

RIP, RNA isolation and RT-qPCR

For RNA co-immunoprecipitations (RIP) ES-2 cell extracts (1×10^7 per condition) were prepared on ice using RIP buffer (10 mM Hepes, 150 mM KCl, 5 mM MgCl₂, 0.5%

NP40, pH 7.0). Cleared extracts were incubated with anti-GFP antibodies and Protein G Dynabeads (Life Technologies) for 30 min at room temperature (RT). After 3 washing steps with RIP buffer, protein-RNA complexes were eluted by SDS. Protein isolation was analyzed by Western blotting. Co-purified RNA was extracted using TRIZOL and analyzed by RT-qPCR analyses as described previously (12). Primers are summarized in Supplementary Table T5.

miTRAP experiments

miTRAP experiments using 3’UTRs of LIN28B, SIRT1 and MAPK6 or MS2 control RNA were essentially performed as described recently (31).

Northern and Western blotting

Northern blotting of small RNAs and semi-quantitative infrared Western blotting were performed as recently described (12). Probes and antibodies are summarized in Supplementary Tables T5 and T7, respectively.

Luciferase reporter assays

Luciferase reporter analyses were performed essentially as previously described (12). Luciferase activity was determined 48 h post-transfection of reporters. Reporters containing a minimal vector-encoded 3’UTR (MCS) served as normalization controls.

RNA sequencing and differential gene expression

Libraries for RNA-sequencing (RNA-seq) were essentially prepared as recently described (31,32). Sequencing was performed on an Illumina HighScan-SQ (IZKF, Leipzig, Germany). Low quality read ends as well as remaining parts of sequencing adapters were clipped off using Cutadapt (V 1.6). For total and small RNA-seq analyses reads were aligned to the human genome (UCSC GRCh37/hg19) using TopHat2 (V 2.0.13; (33)) or Bowtie2 (V 2.2.4; (34)), respectively. FeatureCounts (V 1.4.6; (35)) was used for summarizing gene-mapped reads. Ensembl (GRCh37.75; (36)) or miRBase (V 20; (37)) were used for annotations (see Supplementary Table T1A). Differential gene expression (DE) was determined by edgeR (V 3.12; (38)) using TMM normalization, essentially as described previously ((32); see Supplementary Table T1B).

MicroRNA–target predictions

MultiMiR (V 2.1.1; (39)) was used for the analysis of transcript-specific miRNA-targeting (Supplementary Table T3).

CLIP data analysis and CLIP scores

Publicly available data of significantly enriched CLIP peaks for the listed proteins were derived from indicated studies: a) IGF2BP1-3 (40–42); AGO2 (43–45); c) AGO1-4 (40). Data were obtained from ENCODE, NCBI GEO, CLIPdb and doRiNA. Peak coordinates were mapped to

mRNAs as well as intronic regions of all annotated genes (RefSeq, hg19). To generate the cis-element (5'UTR, CDS or 3'UTR) sorted CLIP score, the number of datasets reporting CLIP hits in the respective element of a mRNA were summed up. For IGF2BP1 (CLIP score range: 0–8) the following data were considered: 1 PAR-CLIP (HEK293), 2 eCLIP (hESCs), 2 eCLIP (HepG2), 2 eCLIP (K562) and 1 iCLIP (K562). For IGF2BP2 (CLIP score range: 0–7) the following data were considered: 2 eCLIP (hESCs), 2 eCLIP (K562), 2 iCLIP (K562) and 1 PAR-CLIP (HEK293). For IGF2BP3 (CLIP score range: 0–6) the following data were considered: 1 PAR-CLIP (HEK293), 1 eCLIP (hESCs), 2 eCLIP (HepG2) and 2 iCLIP (K562). For determining AGO (1–4) CLIP scores in the 3'UTR of indicated mRNAs (CLIP score range: 0–6) the following PAR-CLIP data were considered: HEK293 (3), BC-1 (2) and LCL-35 (1) cells.

Kaplan-Meier and gene expression correlation analyses

Hazardous ratios (HR) for indicated genes and tumor cohorts of serous ovarian carcinoma were determined by the Kaplan-Meier (KM) plotter online tool using 'best cutoff analyses' (www.kmplot.com). Gene expression correlations were analyzed via the R2 platform (<http://hgserver1.amc.nl/cgi-bin/r2/main.cgi>) using the indicated TCGA-provided datasets.

GAEA and GSEA analyses

Gene annotation enrichment analyses (GAEA) of differentially up- or downregulated transcripts (Supplementary Table T1B) were performed using the DAVID functional annotation chart 6.8 (<https://david.ncifcrf.gov/home.jsp>) to identify enriched GO-terms for biological processes (Supplementary Table T1D). Only GO terms containing 10 or more genes were considered. Gene set enrichment analyses (GSEA) were performed with the GSEA-Software (46) using a list of all protein coding genes ranked according to fold changes upon knockdown of the respective IGF2BP.

Cell culture and transfection

Cells were cultured and transfected essentially as described recently (12). SiRNAs used are summarized in Supplementary Table T6. For the depletion of DICER1/DROSHA cells were re-transfected after 3 days and harvested 6 days after the initial transfection.

Spheroid growth, invasion and self-renewal assay

The analyses of 3D spheroid growth and anoikis-resistance were performed as recently described (12). For spheroid invasion assays, 1×10^3 cells (in a 96-well) were used in a Cultrex spheroid invasion assay (Trevigen) according to manufacturer's protocol using DMEM (10% FBS), as previously described (47). Invasion was monitored by bright-field microscopy (Nikon TE-2000-E). The invasion index was determined by the perimeter of the invasive front normalized to sphere body perimeters.

3D-Migration and microscopy

Analysis of single cell 3D migration and microscopy was performed as previously described (12). ES-2 cells were embedded in 1.8 mg/ml or 4 mg/ml Collagen I (Merck Millipore) gel as indicated to generate matrices with varying 'stiffness'.

Animal handling and xenograft assay

Animals were handled according to the guidelines of the Martin Luther University. Permission was granted by a local ethical review committee. For subcutaneous xenograft assays 1×10^5 iRFP-labeled ES-2 cells (stably transduced using iRFP encoding lentiviruses; (22)) were harvested in media supplemented with 50% (v/v) matrigel (Sigma) and injected into the left flank of six week old female immunodeficient athymic FOXN1^{nu/nu} nude mice (Charles River). Mice were held with access to chlorophyll-free food to avoid background noise in iRFP image acquisition. Tumor growth and volume were monitored and measured as recently described (22). For monitoring metastasis, subcutaneous tumors of ketamine/xylazine-anaesthetized mice were removed by surgery 16 days post-injection before the tumor burden exceeded the termination criterion (tumor diameter of 1.5 cm). Primary tumors were imaged and the weight was measured. Resection of primary tumors was validated by iRFP imaging post-surgery. Metastasis formation was monitored by iRFP imaging. Mice were sacrificed when termination criteria were reached or 10 weeks post-surgery without metastasis formation according to ethical guidelines.

RESULTS

IGF2BP paralogues serve distinct roles in ovarian cancer-derived cells

Independent studies reported that the elevated expression of all three human IGF2BP paralogues (IGF2BP1-3) is associated with poor prognosis in ovarian cancer. This was re-evaluated by Kaplan-Meier analyses in 1232 serous ovarian carcinomas using KM plotter combining available datasets to a multi-centric study (48). Elevated IGF2BP1 and 3 mRNA expression was significantly associated with reduced overall survival (OS) supporting previous findings (Supplementary Figure S1A (17,29)). Significant association of upregulated mRNA expression with reduced progression free survival (PFS) probability was only observed for IGF2BP1. Surprisingly, the expression of IGF2BP3 was significantly associated with a better PFS prognosis. This trend was even enhanced when analyzing p53-mutated serous ovarian carcinomas. For ovarian cancer, these observations suggested that: (a) IGF2BPs are associated with partially distinct patient prognosis; (b) IGF2BP1 and 3 synthesis is associated with a poor prognosis irrespective of disease progression (OS); c) IGF2BP1 synthesis is associated with a higher risk of disease progression (PFS), in particular in p53-mutated tumors.

To test if IGF2BP paralogues also serve distinct roles in ovarian cancer-derived cells, five tumor cell properties collectively referred to as 'oncogenic tumor cell properties' were monitored upon the paralogue-specific depletion

of IGF2BPs using siRNA pools (Figure 1A and B). ES-2 cells were used for these studies since they are considered suitable models for studying serous ovarian cancer *in cellulo* (49), express all three IGF2BPs (Figure 1A and B; Supplementary Figure S1B) and harbor p53 mutations. Moreover, independent studies used these cells for analyzing the role of IGF2BP paralogues (12,17,30). Only the depletion of IGF2BP1 significantly reduced the viability of 2D-cultured ES-2 cells (Figure 1C). The viability and size (quantification not shown) of ES-2 spheroids was significantly decreased by the knockdown of IGF2BP1 (Figure 1D), as previously demonstrated (12). In contrast, spheroid viability remained unaffected by IGF2BP2 depletion and was even significantly enhanced at reduced IGF2BP3 levels. Anoikis-resistance, analyzed at reduced FBS concentration (1%) and low adhesion conditions, was significantly impaired by the knockdown of IGF2BP1 and 2 but remained largely unaffected by the depletion of IGF2BP3 (Figure 1E). In elastic 3D-collagen matrices, only the knockdown of IGF2BP1 severely impaired the speed and distance of single cell migration supporting previous reports indicating that IGF2BP1 promotes tumor cell migration (Figure 1F; Supplementary Movie M1; (12,19)). Consistent with impaired migration, the knockdown of IGF2BP1 essentially abolished the invasion of ES-2 spheroids in 3D-matrigel matrices (Figure 1G). Spheroid invasion was modestly reduced by IGF2BP2 depletion and slightly enhanced by the knockdown of IGF2BP3. To exclude potential bias by siRNA-dependent off-target effects, three of the investigated phenotypes were analyzed upon the CRISPR/CAS9-directed deletion of IGF2BP1 or 3 in ES-2 cells (Supplementary Figure S1C). The loss of IGF2BP1 severely impaired the viability of spheroids, anoikis resistance and spheroid invasion (Figure 1H–J). The deletion of IGF2BP3 modestly enhanced spheroid viability whereas anoikis resistance and spheroid invasion remained largely unaffected. To test if the re-expression of IGF2BP1 restores oncogenic tumor cell properties, spheroid invasion was analyzed in IGF2BP1-deleted ES-2 cells that stably express GFP, GFP-IGF2BP1 or a RNA-binding deficient GFP-IGF2BP1 (GFP-I1mut) mutant (12,50). In comparison to GFP or GFP-I1mut expressing cells, invasion was significantly increased by GFP-IGF2BP1 indicating that the phenotypic effects observed by depletion or deletion unlikely result from off-target effects (Supplementary Figure S2A). To determine if the forced expression of IGF2BPs promotes tumor cell phenotypes, the migration speed of ES-2 cells in stiff 3D-collagen I matrices (4mg/ml) was monitored upon IGF2BP overexpression (Supplementary Figure S2B; Supplementary movie M2). In contrast to the forced expression of IGF2BP2 or 3, GFP-IGF2BP1 significantly enhanced 3D-migration speed. This increase was severely reduced by the depletion of exogenous (siRNA: GFP) as well as total IGF2BP1 (siRNA: I1). Intrigued by these findings spheroid growth, anoikis resistance and invasion were analyzed by the overexpression of GFP-IGF2BP1 (Supplementary Figure S2C–E). All three phenotypes were significantly enhanced by the forced expression of IGF2BP1 indicating that the protein enhances an ‘aggressive’ ES-2 tumor cell phenotype.

IGF2BP1 deletion impairs tumor growth in nude mice

Aiming to test if the deletion of IGF2BP1 also impairs tumorigenesis *in vivo*, control (parental) and IGF2BP1-deleted ES-2 cells were transduced with lentiviral vectors encoding iRFP (near-infrared fluorescent protein). This allows monitoring the growth of *Xenografts* by non-invasive near-infrared imaging, as previously described (22).

To determine how IGF2BP1 deletion affects tumor growth, 1×10^5 ES-2 cells were injected subcutaneously (*sc*) in the left flank of female *Foxn1^{mut}* mice. The analysis of tumor size demonstrated that tumor growth was significantly delayed for ES-2 cells lacking IGF2BP1 (Figure 2A and B). All tumors were isolated when the first tumors reached a tumor diameter of ~ 1.5 cm (termination criterion). This endpoint analysis confirmed that tumor volume and mass were substantially reduced by IGF2BP1 deletion indicating that the loss of IGF2BP1 interferes with tumor growth *in vivo* (Figure 2C–E).

IGF2BP1’s phenotypic roles *in cellulo*, in particular enhanced migration and invasion, suggested that the protein also promotes metastasis. Even though metastasis of *sc* tumors derived from ovarian cancer cells appeared unlikely, metastasis was monitored after the resection of primary tumors (Figure 2F). Complete resection of primary *sc* tumors was confirmed by infrared imaging after surgery. Starting ~ 2 weeks after surgery, metastases were observed in two of five control mice (ES-2 parental cells) that survived surgery. Metastases were found at the *pleura* (data not shown) and/or at the residual thymus. In contrast, up to 10 weeks after surgery no metastases were observed in four surviving animals that were injected with IGF2BP1-deleted ES-2 cells (sgI1) initially. Although remaining preliminary, these findings provide strong evidence that the deletion of IGF2BP1 interferes with the ‘metastatic potential’ of ES-2 cells in nude mice. This is consistent with the observation that IGF2BP1 promotes the migratory and invasive potential of ES-2 cells *in vitro* and that IGF2BP1 expression is associated with poor overall and progression free survival in ovarian cancer.

Conservation of oncogenic roles of the IGF2BP family in cancer-derived cells

All three IGF2BPs were reported to promote ‘oncogenic’ properties of tumor cells derived from distinct solid cancers. To investigate the phenotypic conservation of IGF2BP paralogues in cancer cells, two phenotypes (spheroid growth and anoikis resistance) were analyzed in four additional cancer-derived cell lines: OVCAR-3 (ovarian carcinoma), MV-3 (melanoma), A549 (lung adenocarcinoma) and HepG2 (Hepatocellular carcinoma, HCC). Only the depletion of IGF2BP1 impaired both cell properties, in all analyzed tumor-derived cells (Figure 3A–C, blue). The knockdown of IGF2BP2 significantly interfered with spheroid growth and anoikis resistance in HepG2 cells and anoikis resistance in A549 cells (Figure 3A–C, light gray). Spheroid growth and anoikis resistance were impaired by IGF2BP3 depletion only in A549 cells (Figure 3A–C, dark gray), supporting a recently reported role of this paralogue in lung cancer (51). In melanoma-derived MV-3 cells, the knockdown of IGF2BP3 led to enhanced spheroid growth.

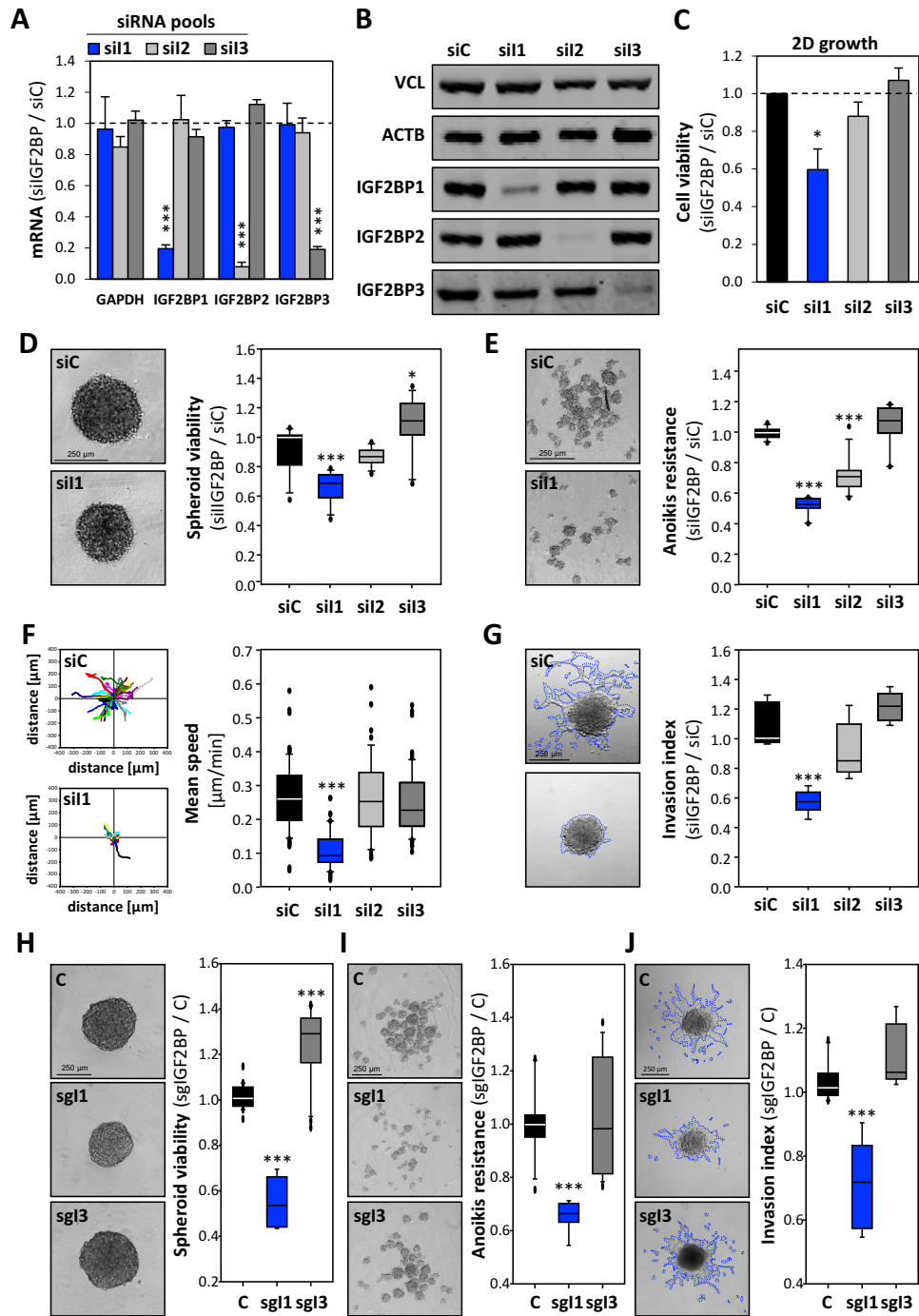


Figure 1. Phenotypic roles of IGF2BPs in ovarian cancer-derived cells. (A) RT-qPCR analysis of paralogue-specific IGF2BP depletion (72 h) using siRNA pools in ES-2 cells. ACTB mRNA levels served as normalization control. (B) Representative Western blot analysis of knockdown analyses shown in (A). VCL and ACTB served as loading controls. (C, D) The viability of ES-2 cells in a 2D cell culture system (C) or ES-2 derived spheroids cultured at 10% FBS in concave ultra-low attachment plates (D) was determined by Cell-titer GLO (Promega) 72h post-transfection with indicated siRNA pools. Cells transfected with control siRNA (siC) served as control and the median viability was set to one. (E) Anoikis-resistance and self-renewal potential of ES-2 cells was determined relative to controls (median set to one) by Cell-titer GLO 6 days post-transfection with siRNA pools. Cells were cultured in planar ultra-low attachment plates at 1% FBS. (F) Single cell migration of ES-2 cells in 3D collagen matrix (1.8 mg/ml) was determined over 10h starting ~60 h post-transfection of indicated siRNA pools. The distance (left panel) and mean speed (right panel) of single cell migration was analyzed in total projections of acquired z-stack image series. Data for at least 40 single cell tracks per condition are shown. (G) The invasive potential of ES-2 spheroids in 3D matrigel matrix was analyzed 72 h post-transfection of indicated siRNA pools. The relative invasion index (median of controls set to one) was determined by the perimeters of the invasive front (traced by blue dashed line) normalized to spheroid body perimeter. (H–J) The spheroid viability (H), anoikis-resistance (I) and spheroid invasion (J) of IGF2BP1- (sg1) or IGF2BP3- (sg3) ES-2 cells were determined (average of two clones) as described in D, E and G, respectively. Parental ES-2 cells served as control. Representative images (D, E, G, H–J) or cell trajectories (F) of controls (siC, knockdown; C, parental ES-2), si1-transfected, IGF2BP1- (sg1) or IGF2BP3- (sg3) ES-2 cells are shown in left panels. Statistical significance was determined by Student's *t*-test; **P* < 0.05; ****P* < 0.001.

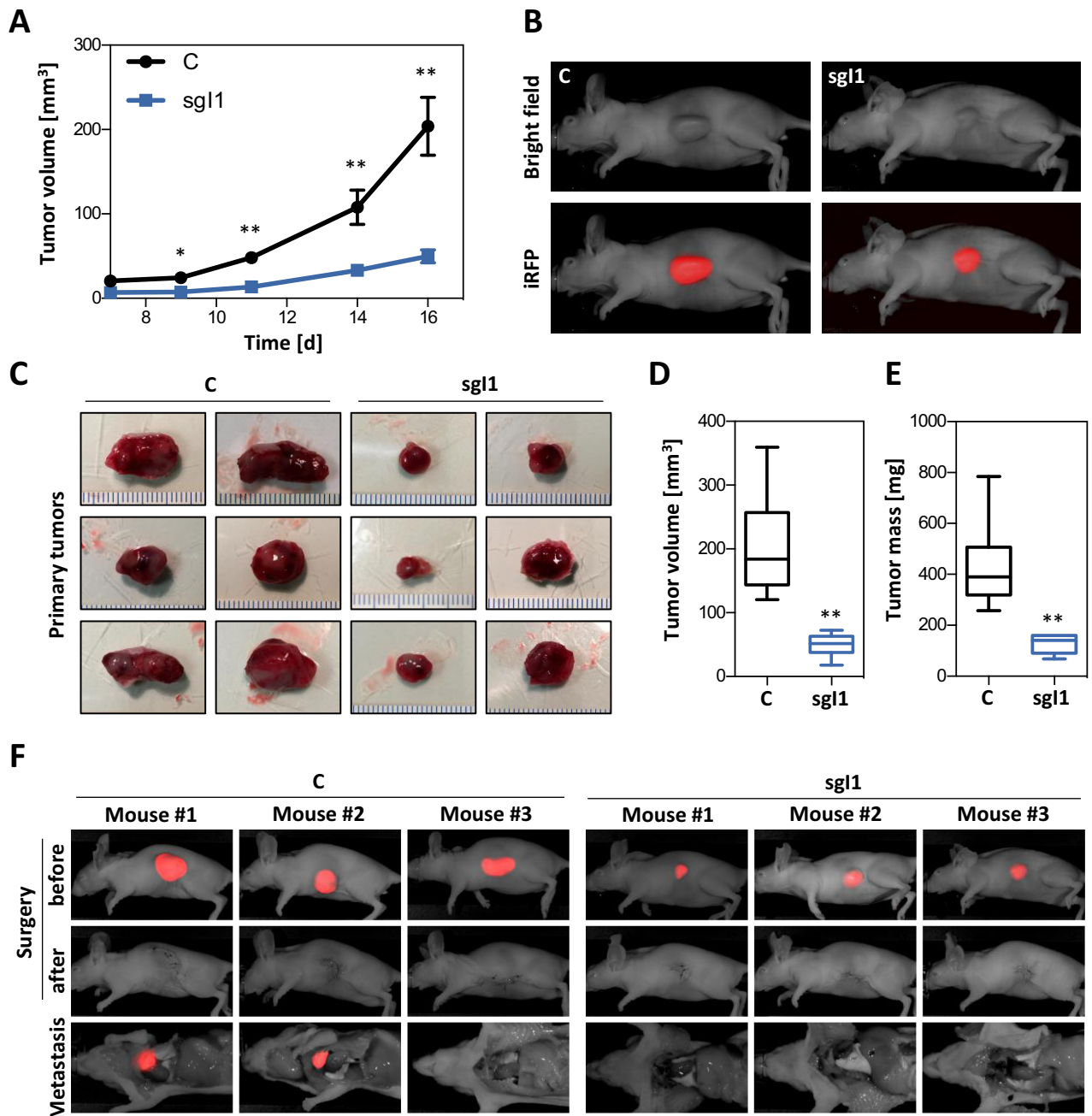


Figure 2. The deletion of IGF2BP1 in ES-2 cells impairs tumor growth and metastasis formation *in vivo*. Control (C) or IGF2BP1-deleted (sg11) ES-2 cells were stably transduced with iRFP-encoding lentiviral vectors and injected into the left flank of female nude mice ($n = 6$ for each condition) to induce the formation of heterologous *Xenograft* tumors. (A) The tumor volume was measured at indicated time points post-injection by a caliper. Error bars indicate standard error of mean (SEM). (B) Representative images of macroscopic tumors acquired by bright field (upper panel) or non-invasive infrared imaging (lower panel) are shown 16d post-injection. (C) Images of primary tumors removed by surgery when the first tumors reached the termination criterion. (D, E) The volume (D) and weight (E) of removed primary tumors were determined and depicted by boxplots. (F) Representative images of three mice are shown before (upper panel) and after (middle panel) surgery. Distant metastases observed in control animals (injected with parental ES-2 cells) are shown in the lower panel using invasive infrared imaging. The standard error of mean (SEM) is shown in (A). Statistical significance was determined by Mann-Whitney's test; * $P < 0.05$; ** $P < 0.01$.

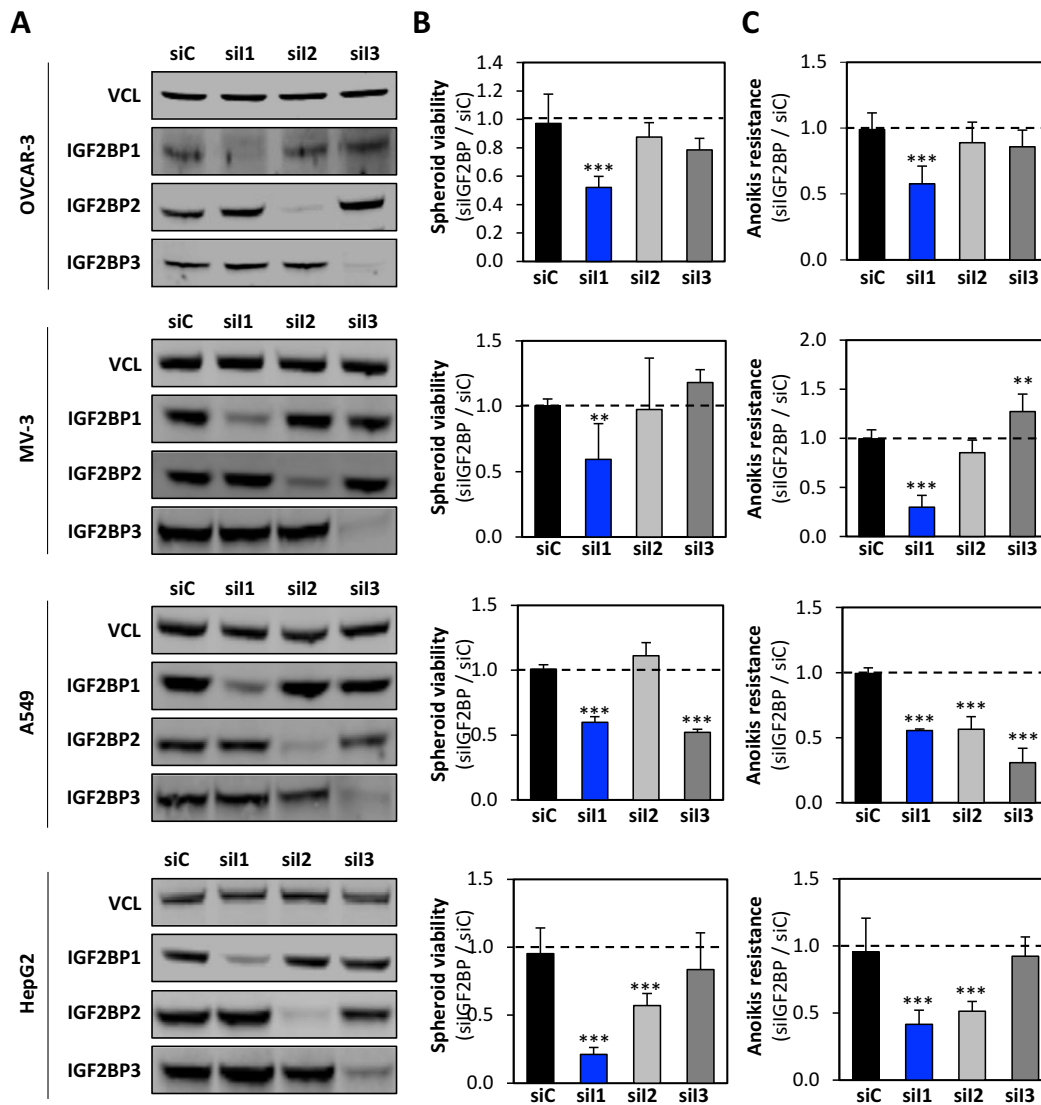


Figure 3. Conservation of IGF2BPs' phenotypic roles in cancer-derived cells. (A) Representative Western blot analysis of paralogue-specific IGF2BP depletion (72 h) using siRNA pools in ovarian cancer-derived OVCAR-3 cells, melanoma-derived MV3 cells, lung cancer-derived A549 cells and HCC-derived HepG2 cells. VCL served as loading control. (B, C) The viability of spheroids and Anoikis resistance of indicated cell lines transfected with control (siC) or siRNA pools targeting indicated IGF2BP paralogues was determined as described in Figure 1B, C. Statistical significance was determined by Student's *t*-test; ***P* < 0.01; ****P* < 0.001.

In summary, these findings indicate that IGF2BP1's phenotypic role in cancer-derived cells is largely conserved whereas the role of IGF2BP2 and 3 varies in a cancer cell-dependent manner.

IGF2BP depletion impairs the expression of partially distinct mRNA panels

Previous studies largely agree that one major role of IGF2BPs is the control of mRNA turnover (15,16). The partially diverse phenotypic roles of IGF2BP paralogues observed in cancer-derived cells, however, suggested that IGF2BPs modulate partially distinct (m)RNA targets. This was addressed by monitoring gene expression upon the paralogue-specific depletion of IGF2BPs in ES-2 cells using RNA-sequencing.

The knockdown of IGF2BPs affected the abundance of mRNAs to varying extent whereas miRNA and lncRNA abundance were only modestly changed (Supplementary Figure S3A–I; Supplementary Table T1A and B). This indicated that IGF2BPs mainly regulate the abundance of mRNAs. To reveal gene sets or pathways regulated by the IGF2BP-dependent control of mRNA abundance gene set enrichment analyses (GSEA) were performed. These identified partially overlapping 'pathway gene sets' for all three IGF2BPs including MYC target genes, epithelial-to-mesenchymal transition (EMT) and KRAS signaling (Figure 4A; Supplementary Table T1C). The identification of these pathways is supported by previously reported roles of IGF2BPs. For instance, IGF2BP1 was shown to promote MYC expression, promotes a mesenchymal tumor cell phenotype and shows cross-talk with KRAS signal-

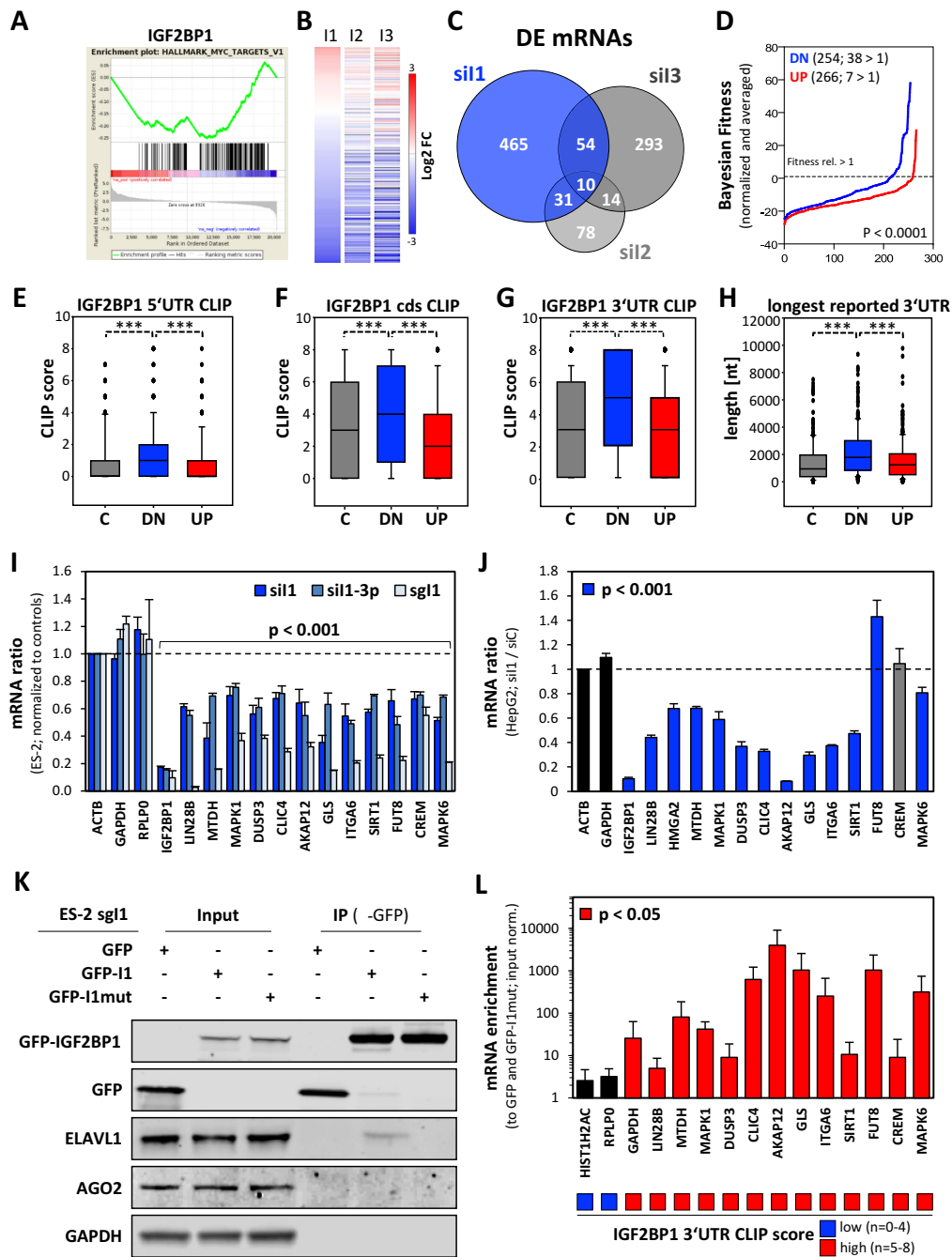


Figure 4. Control of mRNA expression by IGF2BPs in ES-2 cells. (A) Enrichment plot for the pathway gene set 'MYC_TARGETS_V1' determined by gene set enrichment analysis (GSEA) of mRNA expression changes observed upon IGF2BP1 depletion (72 h) in ES-2 cells. (B) Heatmap indicating the \log_2 fold change in expression (FPKM) observed for the 'MYC_TARGETS_V1' gene set upon the depletion of IGF2BP1 (I1), IGF2BP2 (I2) or IGF2BP3 (I3) in ES-2 cells. (C) Venn diagram showing the number and overlap of mRNAs with significant (FDR < 0.1) differential expression (DE) upon the paralogue-specific depletion of IGF2BPs. (E-G) The IGF2BP1 CLIP scores determined in the 5'UTR (E), CDS (F) or 3'UTR (G) of mRNAs significantly down- (DN, blue; 272), upregulated (UP, red; 288) or unchanged (C, 280, gray) are depicted by box plots. (H) The length of the longest reported 3'UTR of mRNAs shown in (E-G) are shown by box plots. (I) Differential expression of indicated mRNAs was determined relative to controls (siC for depletion; parental ES-2 cells for deletion) by: a) RT-qPCR upon IGF2BP1 depletion using siRNA pools (siI1); b) RT-qPCR upon IGF2BP1 depletion using a 3'UTR-directed siRNA (siI1-3p) not included in the pool (a); c) RT-qPCR in response to IGF2BP1-depletion (sgI1) in ES-2 cells. GAPDH and RPLP0 mRNAs served as negative controls. (J) Differential expression of indicated mRNAs upon IGF2BP1 depletion (siRNA pool) in HepG2 cells was determined by RT-qPCR. GAPDH served as negative control. ACTB served as normalization control in both (I, J) RT-qPCR analyses. (K, L) The co-purification of proteins (K) and mRNAs (L) was determined in IGF2BP1-deleted cells expressing GFP, GFP-IGF2BP1 (GFP-I1) or an RNA-binding deficient IGF2BP1 (GFP-I1mut) using immunoprecipitation (IP) by anti-GFP antibodies. Indicated proteins were analyzed by Western blotting (K) in Inputs and upon IP. GAPDH served as negative control. The co-purification of mRNAs was determined by RT-qPCR analyses (L). The enrichment of indicated mRNAs with GFP-IGF2BP1 was determined relative to the co-purification of mRNAs with GFP and GFP-I1mut upon input normalization. RPLP0 and HISTH2AC served as negative controls. The IGF2BP1 3'UTR CLIP score of indicated mRNAs is shown by a heatmap (lower panel). Statistical significance was determined by Student's *t*-test; ****P* < 0.001.

ing (17,52,53). Closer inspection of the mRNAs denoted as leading edge subset by the GSEA application revealed a substantial overlap of transcripts deregulated upon the depletion of IGF2BP paralogues (Supplementary Figure S4A, D and G). Pearson correlation analyses revealed that the fold change of mRNA abundance determined for transcripts comprised in the respective gene sets was significantly correlated upon the depletion of IGF2BP paralogues (Supplementary Figure S4B, E and H). The strongest association with correlation coefficients between 0.76–0.8 was observed for the ‘MYC_TARGETS_V1’ gene set. Transcripts comprised in this gene set were mostly downregulated by the depletion of IGF2BPs supporting a role of IGF2BPs in promoting MYC expression. However, in ES-2 cells only the depletion of IGF2BP1 and 2 reduced MYC protein levels (Supplementary Figure S4J). In contrast, MYC protein abundance was modestly increased by the depletion of IGF2BP3 suggesting distinct regulation of MYC target gene expression by this paralogue. Like observed for MYC, IGF2BP paralogues regulated KRAS mRNA levels to varying extent (Supplementary Figure S4K). These findings suggested that IGF2BPs control similar ‘pathway gene sets’ but regulate mRNA abundance in a largely paralogue-dependent manner. This was supported by four observations: (i) IGF2BPs controlled the abundance of mRNAs comprised in the evaluated ‘pathway gene sets’ in a distinct manner (Figure 4B; Supplementary Figure S4C, F and I); (ii) The number of mRNAs showing significantly (FDR < 0.1) changed expression upon the depletion of every single IGF2BP was rather small (Figure 4C); (iii) The knockdown of IGF2BP1 had the most prominent effect on the differential expression (DE) of mRNAs supporting its comparatively ‘strong’ phenotypic role in ES-2 cells (Figure 4C); (iv) Gene annotation enrichment analyses (GAEA) of mRNAs showing significant DE indicated a substantial paralogue-dependent diversity (Supplementary Figure S5A and Table T1D). For IGF2BP1, GAEA showed a significant enrichment of cell migration-associated genes among downregulated (DN) transcripts. In contrast, cell death-associated mRNAs were significantly enriched among DN transcripts upon IGF2BP3 knockdown. This was in good agreement with phenotypic effects observed in ES-2 cells and suggested that prime effector mRNAs of IGF2BPs are comprised among DN transcripts. This hypothesis was evaluated further by analyzing the tumor cell fitness relevance of DE transcripts (54). Cell fitness relevance, indicated by a Bayesian factor greater one or elevated fitness scores, was significantly higher for DN transcripts when compared to mRNAs upregulated (UP) upon IGF2BP1 depletion (Figure 4D; Supplementary Figure S5B and C). Although less prominent, this trend was also observed for the other two IGF2BP paralogues.

Aiming to identify target mRNAs regulated directly by IGF2BP1, the conservation of CLIP (cross-linking immunoprecipitation) sites reported for DE transcripts in HEK293 (PAR-CLIP; (40)), human pluripotent stem cells (eCLIP; (42)), leukemia-derived K562 and HCC-derived HepG2 cells (eCLIP and iCLIP; (41)) was determined (Supplementary Table T2). This strategy settled on the observation that IGF2BP1’s phenotypic roles were largely conserved among tumor-derived cells suggesting that func-

tionally relevant protein-RNA associations are conserved as well. To allow for a rapid and comprehensive genome wide view of IGF2BP1-CLIP data derived by distinct techniques and analysis strategies, identical CLIP-site positions in 5’UTRs, coding sequences (CDS) and 3’UTRs were determined by considering eight data sets (40–42). The overlay of CLIP sites revealed candidate hot spots of IGF2BP1-association in target mRNAs, for instance the LIN28B 3’UTR (Supplementary Figure S6A; (12)). To rate CLIP-reported mRNA-binding, the CLIP score (CS) indicating the number of experiments demonstrating binding of IGF2BP1 in the 5’UTR, CDS and 3’UTR of specific mRNAs was determined. For the LIN28B 3’UTR, IGF2BP1-binding was reported in all of the eight considered analyses indicating the maximum CS of eight and thus a high conservation of this protein-mRNA association. The genome wide analysis of IGF2BP1’s CLIP scores confirmed preferential binding to mRNAs and identified the 3’UTR as the preferentially bound cis-element, as previously reported (Supplementary Figure S6B, C; (40)).

The analysis of transcripts differentially expressed upon IGF2BP1 depletion in ES-2 cells revealed significantly elevated CLIP scores for the 5’UTRs, CDSs as well as 3’UTRs of DN (272) mRNAs when compared to UP (288) or control (C, 280; randomly selected) transcripts (Figure 4E–G). The largest median CS was determined for 3’UTRs and the median length of the longest reported 3’UTR of mRNAs was significantly elevated among DN mRNAs (Figure 4H). Based on PAR-CLIP (40) and RNA Bind-n-Seq (42) analyses, AC-rich RNA-binding motifs were suggested for IGF2BP1. All of these were significantly increased in the 3’UTRs (normalized to 3’UTR length) of DN transcripts (Supplementary Figure S6D–H). This was not observed for a GU-rich control motif providing further evidence that IGF2BP1 preferentially associates at the 3’UTR of its DN target mRNAs. Significantly increased CLIP scores were also observed for mRNAs significantly downregulated upon IGF2BP2 or 3 depletion suggesting that all three IGF2BPs promote the abundance of target mRNAs in a preferentially 3’UTR-dependent manner (Supplementary Figure S7A–C).

To validate regulation by IGF2BP1 and test if the conservation of CLIP sites is a valid indicator for mRNA association, 11 DN transcripts with an IGF2BP1 3’UTR CS greater than four were selected for further analyses. In ES-2 cells, all these mRNAs and the recently reported target mRNA LIN28B, serving as positive control, were downregulated upon IGF2BP1 deletion (sgI1) and its depletion using a 3’UTR-directed siRNA (siI1-3p) not comprised in the siRNA pool (Figure 4I). With the exception of two mRNAs (FUT8 and CREM), all selected DN mRNAs were also decreased by the depletion of IGF2BP1 in HCC-derived HepG2 cells (Figure 4J). This indicated that the conservation of IGF2BP1’s phenotypic roles is associated with substantially conserved regulation of mRNA fate. Next, the association of proteins and mRNAs was analyzed in ES-2 cells using RIP. To this end, co-purification was determined in IGF2BP1-deleted ES-2 cells expressing GFP-IGF2BP1 (GFP-I1), RNA-binding deficient IGF2BP1 (GFP-I1mut; (50)) or GFP. The RNA-binding protein HuR (ELAVL1) was only co-purified with wild type IGF2BP1 confirm-

ing the RNA-dependent association of both proteins (Figure 4K; (50)). No association was observed for GAPDH (negative control) or AGO2 suggesting that IGF2BP1 does neither associate with RISC factors nor RISC-associated mRNAs. The analysis of input-normalized mRNA enrichment revealed that all 11 DN mRNAs and LIN28B were selectively enriched with GFP-IGF2BP1 when compared to GFP or GFP-I1mut (Figure 4L). Two transcripts with low CLIP scores (HIST1H2AC and RPLP0) served as negative controls. Finally, the abundance of DN mRNAs in IGF2BP1-deleted ES-2 cells re-expressing GFP-IGF2BP1 was compared to cells expressing GFP or GFP-I1mut (Supplementary Figure S7D). In contrast to largely unaffected controls (HIST1H2AC and RPLP0), the abundance of all (except CREM) DN transcripts was significantly increased by wild type IGF2BP1. This showed that IGF2BP1 re-expression restored target mRNA levels in a RNA-binding dependent manner and thus largely excluded bias by off-target effects. In summary, these findings indicate that IGF2BP1 promotes the abundance of target mRNAs by associating with these transcripts and other RBPs, e.g. HuR, in AGO2 and thus RISC-free mRNPs, as previously proposed (12).

Candidate target mRNAs of IGF2BP1 are preferred miRNA targets

IGF2BP1 impairs the miRNA-directed degradation of some target mRNAs, for instance BTRC1 or LIN28B (12,55). If mRNAs deregulated upon IGF2BP1 depletion or deletion in ES-2 cells are prone to miRNA-dependent regulation was first analyzed by predicting miRNA-targeting of DN, UP as well as control transcripts using multiMiR (39). The number of miRNAs showing at least 100 CPM (counts per million mapped transcripts) in ES-2 cells and predicted by at least two of eight databases was significantly increased for DN transcripts (Figure 5A; Supplementary Tables T3 and T4). This was also observed for the abundance of targeting miRNAs in ES-2 cells (Figure 5B). Finally, transcripts deregulated upon IGF2BP1 depletion as well as randomly selected unaffected control mRNAs were analyzed for AGO CLIP sites in their 3'UTR. Assuming that miRNA- and thus RISC-targeting is conserved, as determined for IGF2BP1-binding, five AGO2 and one AGO1-4 CLIP study were investigated (40,43–45). Consistent with increased miR-targeting, AGO-CLIP scores were significantly increased among DN transcripts (Figure 5C). Notably, this was also observed for the other IGF2BP paralogues suggesting that all three IGF2BPs preferentially promote the expression of miRNA-regulated target mRNAs (Supplementary Figure S7A–C). For LIN28B and the 11 selected DN target mRNAs of IGF2BP1 miR-dependent regulation was further on confirmed by elevated mRNA levels determined upon the co-depletion of DICER and DROSHA in ES-2 cells (Figure 5D and E). This was associated with severely reduced miRNA levels, as demonstrated by Northern blotting for let-7a, miR-22 and miR-21, the most abundant miRNA in ES-2 cells (Figure 5D). If IGF2BP1 impairs miRNA-directed downregulation of miR-prone target mRNAs was investigated by comparing mRNA levels upon IGF2BP1 depletion alone and the triple

knockdown of IGF2BP1, DICER and DROSHA (Figure 5D and F). In contrast to controls (ACTB, GAPDH and RPLP0), all analyzed IGF2BP1 target mRNAs were significantly reduced by the knockdown of IGF2BP1 and upregulated by the triple depletion. This was further supported by analyzing LIN28B protein levels (Figure 5D). These were decreased upon the depletion of IGF2BP1 and enhanced by the triple knockdown. Together, this indicated that the IGF2BP1-dependent regulation of miRNA-controlled target mRNAs is strictly miRNA-dependent. Finally, this was evaluated by analyzing the association of mRNAs with AGO2 in control (parental ES-2 cells) and IGF2BP1-deleted ES-2 cells, as previously shown for IGF2BP3 (21). The analysis of proteins co-purified with AGO2 confirmed that IGF2BP1 and AGO2 are not associated in ES-2 cells, as previously shown by IGF2BP1-RIP (Figure 5G; compare to Figure 4K). The analysis of input-normalized mRNA enrichment showed that the AGO2-association of all 12 IGF2BP1 target transcripts was significantly enhanced in cells deleted for IGF2BP1 (Figure 5H). In conclusion, these findings indicate that IGF2BP1 interferes with the miRNA-dependent downregulation of its miR-prone target mRNAs by preventing miRNA/RISC-association.

IGF2BP1 interferes with miRNA-directed decay of the SIRT1 mRNA

Aiming to evaluate if the observed impairment of miRNA-dependent regulation solely relies on the direct coverage of miRNA binding sites (MBS) by IGF2BP1, regulation of the SIRT1 mRNA, one of the novel miR-prone target mRNAs, was analyzed in further detail. The SIRT1 mRNA decayed more rapidly upon the depletion of IGF2BP1 indicating that the protein interfered with SIRT1 mRNA turnover (Figure 6A). The activity of a luciferase reporter comprising the SIRT1 3'UTR was significantly reduced in ES-2 cells deleted for IGF2BP1 (Figure 6B). This was not observed for a control reporter comprising a vector-encoded 3'UTR (MCS) suggesting that IGF2BP1 controls SIRT1 mRNA turnover largely via the 3'UTR. *In silico* predictions of miRNAs targeting the SIRT1 3'UTR and expressed in ES-2 cells with a CPM greater than 100 by multiMiR identified six different miRNAs (Figure 6C). Additionally, seven MBSs for this cis-element were proposed by TargetScan 7.1 (www.targetscan.org). Three (miRs: 155, 22, 140-I) of the seven predicted MBSs overlap with nucleotides (nt) for which CLIP sites were reported by at least two of the eight considered IGF2BP1-CLIP studies. To test the activity and IGF2BP1-dependent regulation of SIRT1-derived MBSs, luciferase reporters comprising the respective MBSs and 20 nt up and downstream of the SIRT1 3'UTR were fused 3' to a luciferase CDS. Compared to a control reporter (MCS), the activity of all seven reporters comprising SIRT1-derived MBSs was significantly reduced in parental ES-2 control cells suggesting miRNA-targeting of all MBSs (Figure 6D, gray). Compared to parental ES-2 cells, the deletion of IGF2BP1 significantly reduced the activity of reporters comprising the SIRT1-derived MBSs with reported IGF2BP1 CLIP sites suggesting coverage of these MBSs (Figure 6D, blue). Finally, the distribution of IGF2BP1-3 as well as AGO2 CLIP sites in the 3'UTR of human

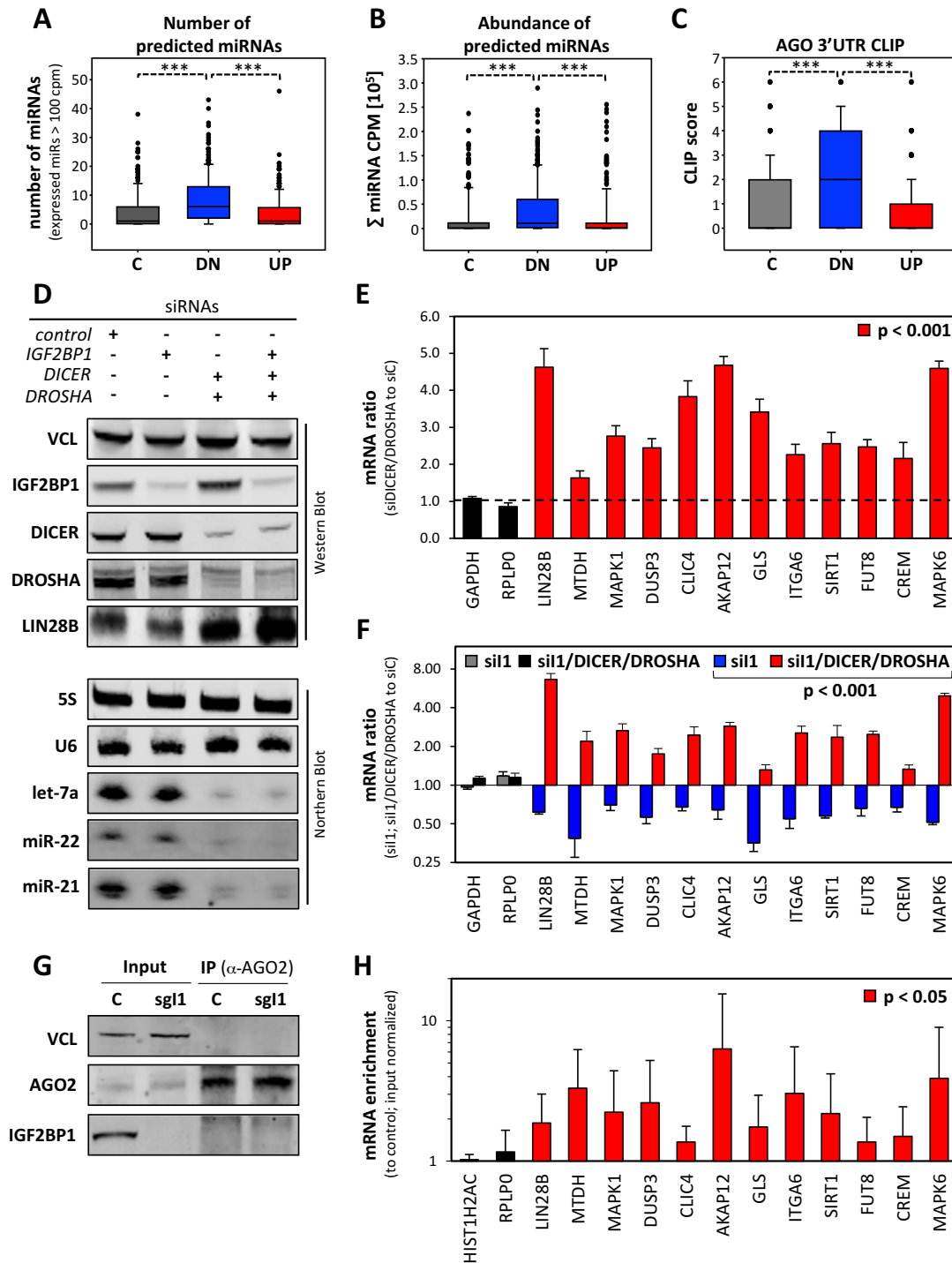


Figure 5. IGF2BP1 target mRNAs are prone to miRNA-dependent regulation. (A, B) The number (A) and summed abundance (B) of miRNAs expressed in ES-2 cells and predicted to target the transcripts analyzed in Figure 4E-H is depicted by box plots. Only miRNAs expressed with a CPM > 100 and predicted (multiMiR) by at least 2 out of 8 databases were considered. (C) The AGO CLIP scores determined for the 3'UTRs of mRNAs analyzed in (A, B) are depicted by box plots. (D) Representative Western blot analysis (upper panel) of indicated proteins upon the depletion of IGF2BP1, DICER and DROSHA co-depletion or triple depletion in ES-2 cells 6d post-transfection (re-transfection after 3d). VCL served as loading control. Representative Northern blot analysis of indicated ncRNAs upon the indicated depletions are shown in the lower panel. 5S and U6 ncRNAs served as loading controls. (E, F) The differential expression of indicated mRNAs upon DICER/DROSHA (E), IGF2BP1 (F, si1) or triple knockdown (F, si1/DICER/DROSHA) was determined by RT-qPCR using ACTB for normalization. GAPDH and RPLP0 served as negative controls. Color coding indicates significance determined by Student's *t*-test. (G, H) The co-purification of proteins (G) and mRNAs (H) with AGO2 in parental (C, control) or IGF2BP1-deleted (sg11) ES-2 cells was determined by immunoprecipitation (IP) using anti-AGO2 antibodies. Indicated proteins were analyzed by Western blotting (G) in Inputs and upon IP. VCL served as loading and negative control. The co-purification of mRNAs was determined by RT-qPCR analyses (H). The enrichment of indicated mRNAs with AGO2 in IGF2BP1-deleted cells was determined relative to parental cells upon input normalization. RPLP0 and HISTH2AC served as negative controls. Statistical significance was determined by Student's *t*-test; ****P* < 0.001.

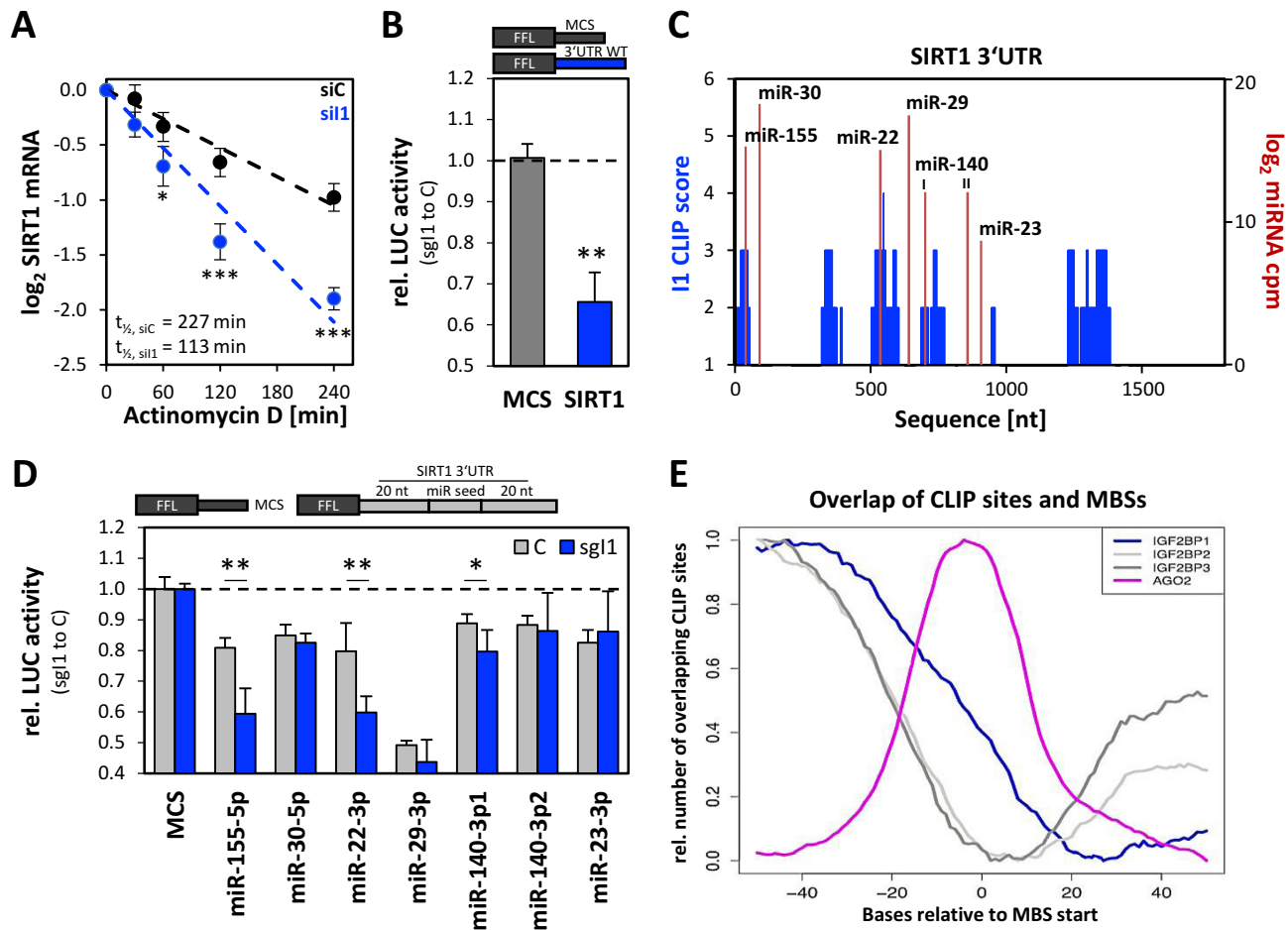


Figure 6. IGF2BP1 interferes with the miRNA-directed decay of the SIRT1 mRNA. (A) The decay of SIRT1 mRNA was monitored by RT-qPCR in IGF2BP1-depleted (si11) or control-transfected (siC) ES-2 cells by blocking mRNA synthesis using actinomycin D (5 μ M) for indicated time points upon normalization to RNA input levels. (B) The activities of a control luciferase-reporter (MCS) and a reporter comprising the 3'UTR of SIRT1 was determined in IGF2BP1-deleted ES-2 cells (sg11) and control cells (C, parental ES-2 cells). Relative (sg11 to C) reporter activity is shown. (C) The number of CLIP studies showing CLIP sites for IGF2BP1 in the SIRT1 3'UTR (left axis, blue) and targeting sites of miRNAs (right axis, red) are shown for the SIRT1 3'UTR at nucleotide-resolution. MiRNA abundance is indicated as log₂ CPM. (D) The activity of luciferase reporters comprising fragments of the 3'UTR of SIRT1 with 20 nt 5' or 3' of MBSs shown in (C) were determined relative to control reporter activity (MCS) in IGF2BP1-deleted cells (sg11, blue) and parental ES-2 cells (C, gray). (E) The relative number of overlapping CLIP sites determined for IGF2BP1-3 or AGO2 in the proximity of MBSs are shown relative to the MBS start sites predicted by TargetScan for human mRNAs (hg19). Statistical significance was determined by Student's *t*-test; **P* < 0.05; ***P* < 0.01; ****P* < 0.001.

mRNAs was compared to predicted MBS positions (Figure 6E). AGO2 CLIP sites tended to overlap with MBS start sites suggesting that the protein preferentially associates in the 5'-vicinity of MBSs. In contrast, IGF2BP CLIP sites were enriched ~40 nucleotides upstream of MBS start sites but showed variable overlap with AGO2-binding regions. Among IGF2BP paralogues, IGF2BP1 CLIP sites showed the most prominent overlap with AGO2 CLIP sites in the 5'-vicinity of MBSs. In contrast to IGF2BP1 and AGO2, binding of IGF2BP2 and 3 was modestly enhanced in the 3'-vicinity of MBSs suggesting similar but distinct binding properties of IGF2BPs in proximity to MBSs. In summary, this suggests that IGF2BPs do not preferentially cover MBSs but partially overlap with AGO2-binding sites.

IGF2BP1 modulates mRNA fate in a miRNome-dependent manner

The IGF2BP1-dependent stabilization of miR-prone target mRNAs was abrogated when miRNAs were depleted implying that IGF2BP1-dependent regulation is miRNome-dependent. This was tested for the validated miR-prone target mRNAs LIN28B, SIRT1 and MAPK6 in ovarian cancer-derived ES-2 and HCC-derived Huh-7 cells. These target mRNAs were chosen since LIN28B and MAPK6 are prone to regulation by the let-7 miRNA family whereas this was neither reported nor predicted for the SIRT1 mRNA (12,56). The latter, however, is regulated by miR-22 and other miRNAs (57). This was validated by miTRAP (miRNA trapping by RNA affinity purification) in ES-2 cells (31). The affinity purification of the MS2-tagged *in vitro* transcribed LIN28B, SIRT1 and MAPK6 3'UTRs from ES-2 cell lysates revealed co-purification of AGO2

and IGF2BP1 proteins indicating miRNA-dependent regulation and IGF2BP1-association (Figure 7A). The analysis of miRNAs co-purified with the respective 3'UTRs by RT-qPCR showed substantial enrichment of the let-7a miRNA only for the LIN28B and MAPK6 3'UTRs (Figure 7B–D). In contrast, miR-22 was co-purified only with the SIRT1 3'UTR. The most abundant miRNA in ES-2 cells, miR-21, was barely enriched with any of the three 3'UTRs. MiRNA-sequencing revealed that both, ES-2 and Huh-7 cells, express miR-22 whereas in contrast to ES-2, Huh-7 cells barely contain let-7 miRNAs (Supplementary Table T4). This was validated by Northern blotting (Figure 7E). In agreement with miRNA levels, the activity of let-7a antisense (as) luciferase reporters remained unchanged in Huh-7 cells whereas their activity was substantially reduced in ES-2 cells (Figure 7F). Compared to control reporters (MCS), the activity of miR-22 as-reporters was severely reduced in both cells and repression was slightly enforced in Huh-7 cells expressing miR-22 at slightly higher levels. In ES-2 cells, the depletion of IGF2BP1 severely reduced the abundance of all three mRNAs whereas the expression of control transcripts (ACTB and GAPDH) remained unchanged (Figure 7G). In Huh-7 cells, the knockdown of IGF2BP1 only reduced SIRT1 mRNA abundance. This was further supported by analyzing protein levels (Figure 7H–K). The abundance of LIN28B, SIRT1 and MAPK6 proteins was reduced upon IGF2BP1 depletion only in ES-2 cells whereas SIRT1 protein was downregulated also in Huh-7 cells. In summary, these findings indicate that the IGF2BP1-dependent regulation of miR-prone target mRNAs is strictly miRNome-dependent and thus can vary in a cell context-dependent manner.

IGF2BP1 controls tumor cell properties by promoting the expression of miRNA-regulated target mRNAs

The presented analyses indicated that IGF2BP1 promotes oncogenic tumor cell properties and that this is associated with the impairment of miRNA-dependent downregulation of its miRNA-controlled target mRNAs. To evaluate if the 12 (including LIN28B) validated 'miRNA-prone' target mRNAs of IGF2BP1 could serve as downstream effectors in promoting an 'aggressive' tumor cell phenotype anoikis resistance, spheroid growth and spheroid invasion were monitored upon their depletion in ES-2 cells using siRNA pools (Figure 8A–C; Supplementary Figure S8A–D). The knockdown of IGF2BP1 served as positive control.

All three tumor cell phenotypes were significantly impaired by the depletion of IGF2BP1 whereas the knockdown of LIN28B only interfered with spheroid invasion. With the exception of one downstream effector, GLS, the knockdown of all analyzed IGF2BP1-target mRNAs impaired at least one of the investigated phenotypes. Notably, we observed variable association of phenotypic effects. For instance, although SIRT1 depletion impaired anoikis-resistance, invasive potential and spheroid viability remained essentially unchanged. Likewise, although the knockdown of AKAP12 interfered with spheroid invasion, anoikis resistance and spheroid viability were essentially unaffected. Intriguingly, invasive potential was influenced by most of the validated downstream effectors support-

ing the view that IGF2BP1 is a post-transcriptional driver of invasive potential and thus likely of metastasis as supported by *in vivo* studies (see Figure 2). Five of the effectors (ITGA6, MAPK1, FUT8, MTDH and MAPK6) significantly modulated all three phenotypes suggesting a pivotal role in 'IGF2BP1-driven' cancers. Most importantly, none of the depletions significantly enhanced any of the analyzed phenotypic effects. In summary, this indicates that the impairment of miRNA-directed downregulation of its target mRNAs is a major role of IGF2BP1 in cancer-derived cells. Moreover, IGF2BP1 obviously acts via pleiotropic downstream effectors indicating that specific phenotypic roles are interfered by more than one effector.

If IGF2BP1 expression is associated with effector expression also in primary cancers was tested by Pearson correlation in primary ovarian cancer (EOC), hepatocellular cancer (HCC), lung adenocarcinoma (LUAD) and skin cutaneous melanoma (SKM) samples (Figure 8D). Data were derived from TCGA-provided RNA-sequencing data. With the exception of DUSP3 all analyzed IGF2BP1 effectors showed co-expression, indicated by positive correlation coefficients (Pearson R), in at least three of the analyzed cancer data sets. The average Pearson correlation coefficient (Figure 8D, trend) confirmed that effector expression is overall positively associated with IGF2BP1 abundance in all four cancers. Finally, the prognostic relevance of effector expression on progression free (PFS) and overall survival (OS) was analyzed by Kaplan Meier studies in serous ovarian carcinomas (SOC) by KM plotter (Figure 8E). IGF2BP1 and LIN28B were identified as the most prominent indicators of a poor prognosis. This is indicated by hazardous ratios (HR) greater than one determined for all analyzed conditions. The highest HR was retrieved for IGF2BP1 in PFS analysis (HR: 2.35; $P = 8.6 \times 10^{-5}$) of p53-mutated SOC. With the exception of MAPK1 and FUT8, elevated expression of all effectors was associated with poor PFS-prognosis in p53-mutated SOC. Consistently, the highest average HR (Figure 8E, trend) was observed for PFS-prognosis in p53-mutated SOC. This was expected since effectors were identified in p53-mutated ovarian cancer-derived ES-2 cells.

DISCUSSION

The depletion of IGF2BPs in five tumor cell lines derived from distinct cancers indicates that IGF2BP paralogues serve partially distinct phenotypic roles. IGF2BPs show similar RNA-binding properties and control partially overlapping pathways. However, the sets of significantly deregulated transcripts upon IGF2BP depletion are mainly divergent. AGO2 as well as IGF2BPs preferentially associate with mRNAs downregulated upon IGF2BP depletion suggesting that IGF2BPs mainly impair the decay of their miRNA-controlled target mRNAs. This is confirmed by the analysis of 12 miRNA-regulated target mRNAs of IGF2BP1. Notably, the vast majority of these mRNAs encode factors promoting the anoikis resistance, spheroid viability and/or spheroid invasion of ovarian cancer-derived cells. In primary cancer, enhanced IGF2BP1 synthesis is associated with the elevated expression of these transcripts. Like IGF2BP1, most of its miRNA-controlled target tran-

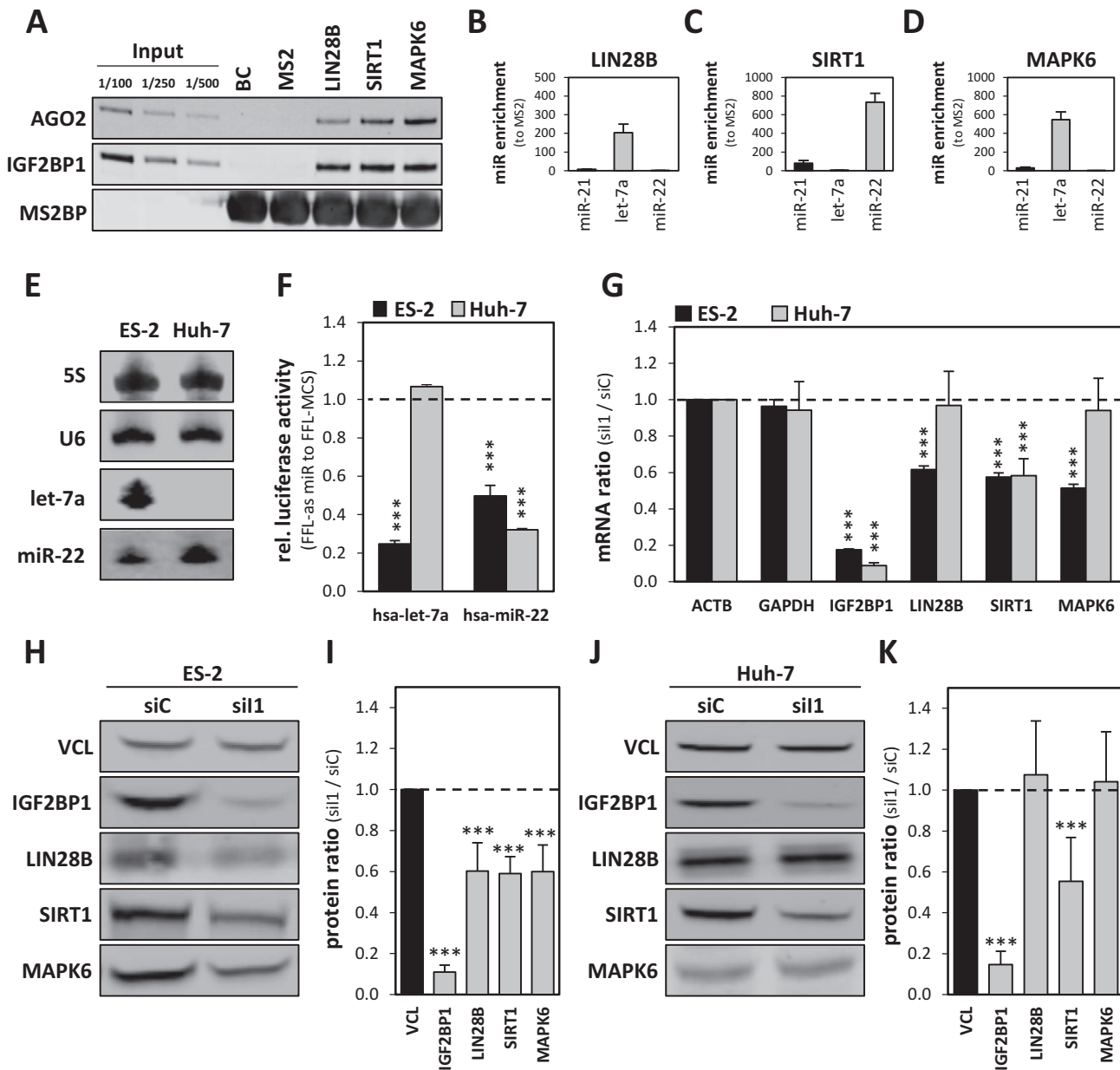


Figure 7. IGF2BP1 modulates target mRNA fate in a miRNome-dependent manner. (A) Representative Western blot analysis of indicated proteins associated with the *in vitro* transcribed 3'UTRs of indicated mRNAs in miTRAP studies (ES-2 cells). MS2BP-coated and MS2/MS2BP-coated amylose resins served as negative controls. Dilutions of protein inputs are shown on the left. (B–D) The association of indicated miRNAs with the 3'UTRs of LIN28B (B), SIRT1 (C) and MAPK6 (D) was determined by miTRAP using RT-qPCR. The enrichment of miRNAs co-purified with 3'UTRs was analyzed relative to MS2 controls. (E) Representative Northern blot analysis of indicated ncRNAs in ES-2 and Huh-7 cells. U6 and 5S RNAs served as loading controls. (F) The activity of let-7 and miR-22 miRNAs in ES-2 and Huh-7 cells was analyzed by miRNA antisense luciferase reporters. The activity of antisense reporters (FFL-as) was normalized to control reporters comprising a vector-encoded 3'UTR (FFL-MCS). (G) RT-qPCR analysis of indicated transcripts upon the depletion of IGF2BP1 in ES-2 and Huh-7 cells. ACTB mRNA levels were used for normalization. GAPDH served as negative control. (H–K) Western blot analysis of IGF2BP1 depletion by siRNA pools (72 h) in ES-2 cells (H, I) and HCC-derived Huh-7 cells (J, K). VCL served as loading and normalization control for determining relative protein ratios in (I, K). Statistical significance was determined by Student's *t*-test; ****P* < 0.001.

scripts indicate poor prognosis in ovarian cancer. Together this indicates that IGF2BP1 enhances an 'aggressive' tumor cell phenotype largely by impairing the downregulation of its miRNA-regulated target mRNAs.

Paralogue-specific roles of IGF2BPs in cancer-derived cells

The analysis of tumor cell phenotypes in a panel of five tumor cells derived from distinct solid cancers indicates that IGF2BP1 has the most conserved 'oncogenic potential' of the IGF2BP family *in cellulo* (Figures 1 and 3; Supplementary Figure S2). This is supported by *Xenograft* studies revealing that the deletion of IGF2BP1 interferes with tumor

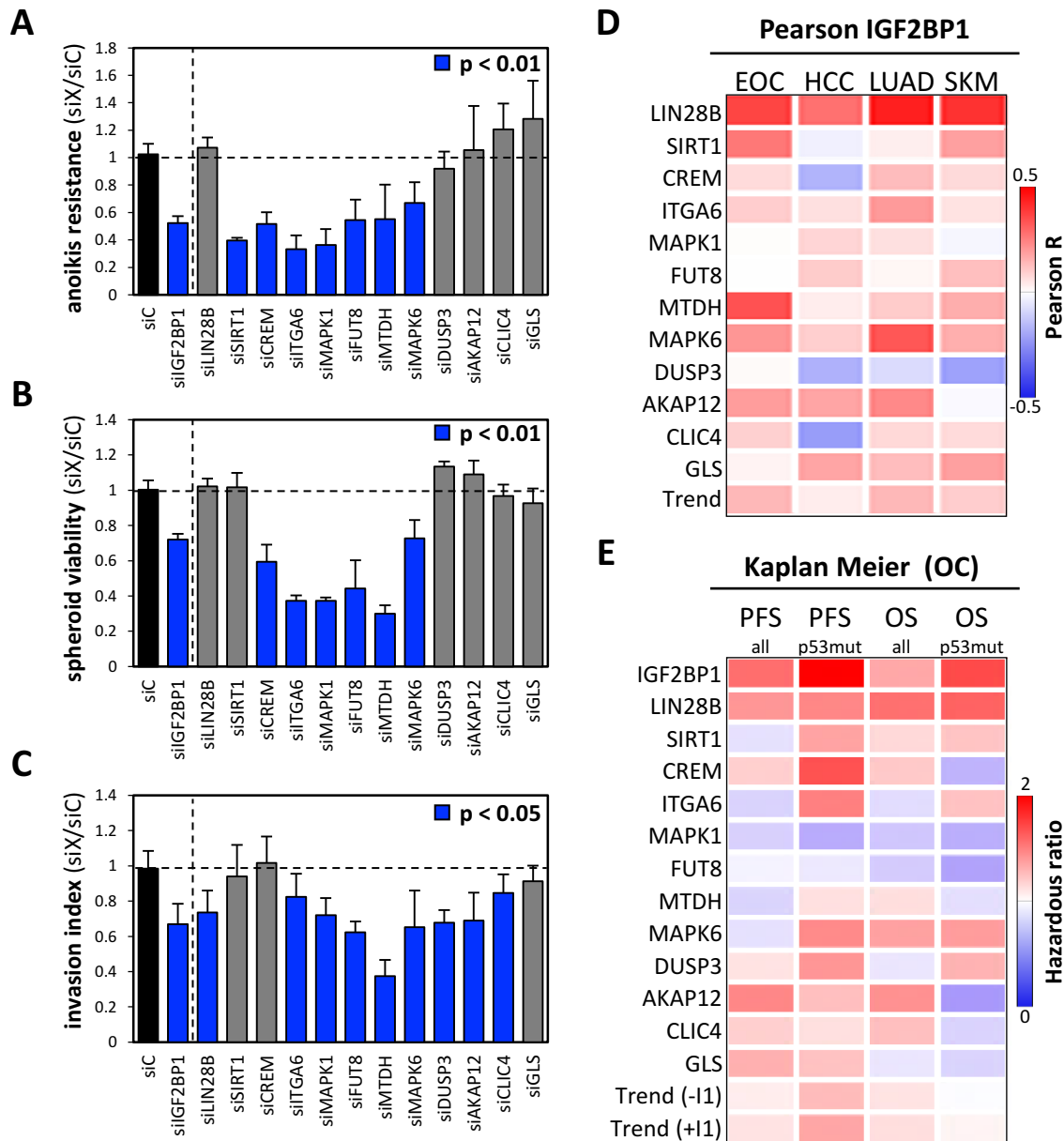


Figure 8. The majority of IGF2BP1’s downstream effectors promote ‘oncogenic’ tumor cell properties. (A–C) The indicated tumor cell properties were monitored in 3D-cultured ES-2 cells 72h post-transfection of siRNA pools directed against indicated target mRNAs, as described in Figure 1. Cells transfected with control siRNA (siC) served as control. The anoikis resistance, spheroid viability and invasion index upon the depletion of indicated factors were determined relative to controls (siC; indicated by dashed line). Statistical significance was determined by Student’s *t*-test and is indicated by color-coding. (D) The co-expression of indicated mRNAs with IGF2BP1 was analyzed by Pearson correlation in TCGA cohorts of ovarian cancer samples (EOC, 304), hepatocellular carcinoma (HCC, 371), lung adenocarcinoma (LUAD, 515) and melanoma (SKM, 470). Pearson correlation coefficients (R) are indicated by a heat map. (E) The hazardous ratio (HR) determined by KM plotter for indicated mRNAs using the best cutoff for indicated conditions in ovarian cancer samples is shown by a heat map. Scale bars for correlations (D) and hazardous ratios (E) are indicated in the right panels.

growth (Figure 2), as previously shown for the depletion of IGF2BP1 in HCC-derived HepG2 cells (22). Upon the resection of primary tumors, metastases were only observed when cells expressed IGF2BP1 (Figure 2). These observations provide strong evidence that the protein promotes metastasis as supported by studies in other cancer models (18,20). The depletion of IGF2BP2 as well as 3 interfered with selected tumor cell phenotypes in some of the analyzed cancer-derived cells indicating that their ‘onco-

genic potential’ varies in a cancer cell-dependent manner. In lung adenocarcinoma- as well as HCC-derived tumor cells (A549 and HepG2), the knockdown of IGF2BP2 impaired spheroid growth and/or anoikis resistance (Figure 3). This supports recent findings indicating that IGF2BP2 enhances the proliferation of tumor cells by promoting the expression of IGF2 and HMGA1 and preserves cancer stem cell phenotypes (24,58). The comparatively moderate conservation of phenotypic effects observed upon IGF2BP3 deple-

tion are surprising in view of the various reports suggesting IGF2BP3 to serve ‘oncogenic’ roles in tumor cells derived from distinct cancers (16). Notably, however, analyses in the five tumor-derived cell lines analyzed here indicate that IGF2BP3 had the most pronounced phenotypic effect of all three IGF2BPs in lung cancer-derived cells (Figure 3). This supports recent studies reporting that IGF2BP3 promotes an ‘aggressive’ phenotype of lung cancer-derived cells by attenuating p53 protein stability (51). This potentially indicates that IGF2BP3 has a partially p53-dependent role in some cancer cells. Except A549 and HepG2 cells all of the tumor cells analyzed here were reported to harbor p53 mutations and/or impaired activity. However, the depletion of IGF2BP3 did not impair the analyzed phenotypes in HepG2 cells suggesting that IGF2BP3-dependent regulation of an ‘aggressive’ tumor cell phenotypes depends on additional yet to determine preconditions. In addition to distinct mutational burden, the observed phenotypic variation is likely associated with substantially distinct IGF2BP paralogue-dependent regulation of mRNA fate. GSEAs that considered differences in transcript abundancies regardless of statistical significance identified mainly the same effector pathways for all three IGF2BPs. However, differential expression of effector transcripts comprised in these pathways varies in a significantly IGF2BP paralogue-dependent manner (Figure 4A and B; Supplementary Figure S4). This suggests that IGF2BPs control partially distinct effector mRNAs, regulate the fate of the same mRNA with varying efficiency and/or control the same mRNA in an opposing manner. Evidence for all these options was observed by comparing differential expression of mRNAs comprised in the GSEA-identified pathways controlled by all three IGF2BPs (Figure 4B; Supplementary Figure S4). Moreover, GAEAs of mRNAs showing significant deregulation upon the paralogue-specific depletion of IGF2BPs suggest partially distinct functions of IGF2BP paralogues based on substantially distinct and paralogue-dependent regulation of mRNA abundance (Supplementary Figure S5A). Despite this variation, all three IGF2BPs preferentially associate with miRNA-targeted mRNAs downregulated upon their depletion suggesting that their main role is the stabilization of target mRNAs (Figure 4E–H; Supplementary Figure S7A–C), as validated here for IGF2BP1 (Figures 4, 5 and 6). Future studies have to characterize the previously proposed variation of RNA-binding properties among IGF2BPs by determining the role of the six RNA-binding domains, two RNA recognition motifs (RRMs) and four HNRNK homology (KH) domains, comprised in all three IGF2BPs (50). Moreover, it needs to be addressed how the relative abundance of IGF2BP paralogues influences their RNA-binding properties and how these are modulated by posttranslational modifications. Together, suchlike studies will likely reveal complex and paralogue-dependent RNA-binding motifs expected in view of up to six partially varying RNA-binding motifs to be considered in IGF2BPs. At the cellular level, future studies need to reveal the conservation of IGF2BP effector transcripts in cancer-derived cells and have to test IGF2BP-dependent regulation of additional phenotypes like metabolic control. This will likely reveal which tumor cell properties are primarily regulated by IGF2BP2 and 3 and which effector

pathways are affected preferentially by these paralogues. Moreover, it remains to be determined if an oncogenic role of IGF2BP2 and 3 is enhanced *in vivo*. *In cellulo* analyses are limited by various means, in particular the lack of tumor-stroma cross-talk. Thus, our studies potentially underestimate the oncogenic potential of IGF2BP2 and 3. With regard of these limitations, the here presented analyses demonstrate that IGF2BP1 has highly conserved oncogenic potential in cancer cells and *in vivo*. These findings indicate that this paralogue is a prime candidate target for therapeutic intervention in distinct solid cancers.

IGF2BP1 promotes an aggressive tumor cell phenotype by ‘safe-guarding’ miRNA-controlled mRNAs

IGF2BPs were reported to control the transport, translation and turnover of mRNAs in the cytoplasm (15). These regulatory roles are partially interconnected, for instance the regulation of ACTB mRNA localization and its spatially restricted translation in developing neurons (59). However, the most frequently reported IGF2BP-dependent regulation in cancer-derived or transformed cells is the stabilization of mRNAs (40), more precisely the impairment of miRNA-directed degradation of IGF2BP target mRNAs (12,21,28,60). An enhancement of (m)RNA decay by IGF2BPs was only suggested for the lncRNA HULC and the IGF2BP3-dependent stimulation of miRNA-targeting of some IGF2BP3-target mRNAs (21,61). The here presented studies indicate that mRNAs downregulated (DN) upon decreased or lost IGF2BP expression are preferentially bound by these RBPs (Supplementary Figure S7A–C). This supports the view that IGF2BPs mainly impair the degradation of mRNAs. Moreover, DN mRNAs show increased AGO-binding and susceptibility to the regulation by microRNAs expressed in tumor-derived cells (Figure 5A–C). The depletion of microRNAs or the lack of miRNA expression, e.g. let-7a in Huh-7 cells, abolished stabilization by IGF2BP1 target mRNAs (Figures 5D–E and 7). This indicates that IGF2BP1 preferentially impairs the miRNA-directed downregulation of effector mRNAs and thus controls the fate of miR-prone mRNAs in a strictly miRNome-dependent manner. In contrast to other studies favoring a direct coverage of miRNA binding sites (MBS) by IGF2BPs (21,24,28), we show here that IGF2BPs barely cover MBSs directly (Figure 6E). Instead they seem to preferentially associate approximately 40 nucleotides upstream of MBSs. Nonetheless, some MBSs are impaired by the binding of IGF2BP1 at or in proximity to the MBS as demonstrated for the IGF2BP1-dependent regulation of SIRT1 expression (Figure 6A–D). Both, direct coverage as well as regulation without MBS-coverage, is also observed for HuR (62). Moreover, this mode of regulation is compatible with the previously proposed ‘safe-guard’ hypothesis (12,28). This does not essentially rely on a direct coverage of MBSs but is also consistent with binding-induced conformational changes at MBSs or the sequestering of target mRNAs in protective mRNPs preventing RISC/miRNA-targeting. The latter appears most plausible since the association of IGF2BP1 with RISC/miRNA-bound mRNAs was neither observed by the immunopurification of IGF2BP1 nor AGO2 (Figures 4K and 5G). Fur-

thermore, previous studies indicated that miRNA-regulated target mRNAs of IGF2BP1 are enriched in RISC/miRNA-free mRNPs (12). At least for IGF2BP1, these observations also argue against an enhancement of miRNA-directed targeting of mRNAs upon IGF2BP1-binding, as proposed for some target mRNAs of IGF2BP3 (21). If this would be observed for at least some mRNAs, it would be expected that IGF2BP1-associated mRNA-protein complexes also comprise RISC components like AGO proteins and miRNAs. This, however, was not observed in this or previous studies (12). Finally, AGO CLIP scores in the 3'UTR of mRNAs upregulated upon IGF2BP1 depletion were significantly smaller than observed for transcripts downregulated at reduced IGF2BP1 levels (Figure 4E–G). Although this was also observed for candidate target mRNAs of IGF2BP2 and 3 (Supplementary Figure S7A–C), future studies are required to clarify if and how these paralogues unlike IGF2BP1 potentially promote RISC/miRNA-association of their miRNA-controlled target mRNA. Conceivable are mechanisms by which IGF2BPs promote RISC/miRNA-association upon binding to target transcripts or indirectly by modulating the abundance of regulators of miRNA-dependent regulation, e.g. other RBPs.

The analysis of selected miRNA-controlled effector mRNAs of IGF2BP1 revealed that their depletion impaired at least one of three analyzed tumor cell phenotypes, with one exception (GLS). Consistently, mRNAs downregulated upon IGF2BP1 depletion were enriched for factors with conserved tumor cell fitness relevance (Figure 4D; (54)). Together this indicates that IGF2BP1 promotes an aggressive tumor cell phenotype largely by impairing the miRNA-dependent downregulation of its effector mRNAs. Although these findings need further investigation, this also appears to be the main role of IGF2BP2 and 3 since tumor cell fitness relevance was likewise increased among mRNAs downregulated by the depletion of these paralogues (Supplementary Figure S5B and C). For IGF2BP1, a role in 'safe-guarding' its miRNA-controlled target mRNAs in primary cancer is further supported by the conserved positive correlation of upregulated expression observed in four primary cancers (Figure 8D). Notably, the cancer cells studied here were derived from the four primary cancer types analyzed in these correlation studies. Thus, the conservation of IGF2BP1's phenotypic roles *in cellulo* is well associated with the co-expression of target mRNAs in the same primary cancer. Finally, elevated expression of IGF2BP1 and its miRNA-regulated effector mRNAs was largely associated with an unfavorable prognosis in p53-mutated serous ovarian carcinomas (Figure 8E). Together this provides strong evidence that the 'safe-guarding' of miRNA-controlled target mRNAs is a major role of IGF2BP1 in tumor cells. Future studies now have to reveal the conservation of this regulation across cancers to develop and evaluate therapeutic strategies aiming at interfering with IGF2BP1-dependent effector networks in cancer.

DATA AVAILABILITY

Total RNA- as well as small RNA-Seq data were deposited at NCBI GEO (GSE109605).

SUPPLEMENTARY DATA

Supplementary Data are available at NAR Online.

ACKNOWLEDGEMENTS

The authors thank Knut Krohn at the Core Unit DNA Technologies IZKF, University of Leipzig for RNA Sequencing and the Core Facility Imaging (CFI) of the Martin-Luther-University for support with all imaging analyses.

Author Contributions: S.M., N.B. and S.H. designed the experiments. S.M., N.B. and B.B. carried out and interpreted the experiments. M.L. and V.R. generated constructs and stable cell populations. T.F. supported the Xenograft analyses. M.G. and D.M. analyzed RNA sequencing data. S.H. conceived the experimental design and wrote the manuscript.

FUNDING

DFG funding [GRK1591, project B3 to S.H.]. Funding for open access charge: Institute budget.

Conflict of interest statement. None declared.

REFERENCES

- Baek,D., Villen,J., Shin,C., Camargo,F.D., Gygi,S.P. and Bartel,D.P. (2008) The impact of microRNAs on protein output. *Nature*, **455**, 64–71.
- Lin,S. and Gregory,R.I. (2015) MicroRNA biogenesis pathways in cancer. *Nat. Rev. Cancer*, **15**, 321–333.
- Hayes,J., Peruzzi,P.P. and Lawler,S. (2014) MicroRNAs in cancer: biomarkers, functions and therapy. *Trends Mol. Med.*, **20**, 460–469.
- Yu,F., Yao,H., Zhu,P., Zhang,X., Pan,Q., Gong,C., Huang,Y., Hu,X., Su,F., Lieberman,J. *et al.* (2007) let-7 regulates self renewal and tumorigenicity of breast cancer cells. *Cell*, **131**, 1109–1123.
- Lee,Y.S. and Dutta,A. (2007) The tumor suppressor microRNA let-7 represses the HMGA2 oncogene. *Genes Dev.*, **21**, 1025–1030.
- Boyerinas,B., Park,S.M., Shomron,N., Hedegaard,M.M., Vinther,J., Andersen,J.S., Feig,C., Xu,J., Burge,C.B. and Peter,M.E. (2008) Identification of let-7-regulated oncofetal genes. *Cancer Res.*, **68**, 2587–2591.
- Sampson,V.B., Rong,N.H., Han,J., Yang,Q., Aris,V., Soteropoulos,P., Petrelli,N.J., Dunn,S.P. and Krueger,L.J. (2007) MicroRNA let-7a down-regulates MYC and reverts MYC-induced growth in Burkitt lymphoma cells. *Cancer Res.*, **67**, 9762–9770.
- Balzeau,J., Menezes,M.R., Cao,S. and Hagan,J.P. (2017) The LIN28/let-7 Pathway in Cancer. *Front. Genet.*, **8**, 31.
- van Jaarsveld,M.T., Helleman,J., Berns,E.M. and Wiemer,E.A. (2010) MicroRNAs in ovarian cancer biology and therapy resistance. *Int. J. Biochem. Cell Biol.*, **42**, 1282–1290.
- Mayr,C. and Bartel,D.P. (2009) Widespread shortening of 3'UTRs by alternative cleavage and polyadenylation activates oncogenes in cancer cells. *Cell*, **138**, 673–684.
- Mayr,C., Hemann,M.T. and Bartel,D.P. (2007) Disrupting the pairing between let-7 and Hmga2 enhances oncogenic transformation. *Science*, **315**, 1576–1579.
- Busch,B., Bley,N., Muller,S., Glass,M., Misiak,D., Lederer,M., Vetter,M., Strauss,H.G., Thomssen,C. and Huttelmaier,S. (2016) The oncogenic triangle of HMGA2, LIN28B and IGF2BP1 antagonizes tumor-suppressive actions of the let-7 family. *Nucleic Acids Res.*, **44**, 3845–3864.
- Powers,J.T., Tsanov,K.M., Pearson,D.S., Roels,F., Spina,C.S., Ebright,R., Seligson,M., de Soysa,Y., Cahan,P., Theissen,J. *et al.* (2016) Multiple mechanisms disrupt the let-7 microRNA family in neuroblastoma. *Nature*, **535**, 246–251.
- van Kouwenhove,M., Kedde,M. and Agami,R. (2011) MicroRNA regulation by RNA-binding proteins and its implications for cancer. *Nat. Rev. Cancer*, **11**, 644–656.

15. Bell, J.L., Wachter, K., Muhleck, B., Pazaitis, N., Kohn, M., Lederer, M. and Huttelmaier, S. (2013) Insulin-like growth factor 2 mRNA-binding proteins (IGF2BPs): post-transcriptional drivers of cancer progression? *Cell. Mol. Life Sci.*, **70**, 2657–2675.
16. Lederer, M., Bley, N., Schleifer, C. and Huttelmaier, S. (2014) The role of the oncofetal IGF2 mRNA-binding protein 3 (IGF2BP3) in cancer. *Semin. Cancer Biol.*, **29**, 3–12.
17. Kobel, M., Weidensdorfer, D., Reinke, C., Lederer, M., Schmitt, W.D., Zeng, K., Thomssen, C., Hauptmann, S. and Huttelmaier, S. (2007) Expression of the RNA-binding protein IMP1 correlates with poor prognosis in ovarian carcinoma. *Oncogene*, **26**, 7584–7589.
18. Craig, E.A., Weber, J.D. and Spiegelman, V.S. (2012) Involvement of the mRNA binding protein CRD-BP in the regulation of metastatic melanoma cell proliferation and invasion by hypoxia. *J. Cell Sci.*, **125**, 5950–5954.
19. Stohr, N., Kohn, M., Lederer, M., Glass, M., Reinke, C., Singer, R.H. and Huttelmaier, S. (2012) IGF2BP1 promotes cell migration by regulating MK5 and PTEN signaling. *Genes Dev.*, **26**, 176–189.
20. Hamilton, K.E., Noubissi, F.K., Katti, P.S., Hahn, C.M., Davey, S.R., Lundsmith, E.T., Klein-Szanto, A.J., Rhim, A.D., Spiegelman, V.S. and Rustgi, A.K. (2013) IMP1 promotes tumor growth, dissemination and a tumor-initiating cell phenotype in colorectal cancer cell xenografts. *Carcinogenesis*, **34**, 2647–2654.
21. Ennajdaoui, H., Howard, J.M., Sterne-Weiler, T., Jahanbani, F., Coyne, D.J., Uren, P.J., Dargyte, M., Katzman, S., Draper, J.M., Wallace, A. *et al.* (2016) IGF2BP3 modulates the interaction of invasion-associated transcripts with RISC. *Cell Rep.*, **15**, 1876–1883.
22. Gutschner, T., Hammerle, M., Pazaitis, N., Bley, N., Fiskin, E., Uckelmann, H., Heim, A., Grobota, M., Hofmann, N., Geffers, R. *et al.* (2014) Insulin-like growth factor 2 mRNA-binding protein 1 (IGF2BP1) is an important protumorigenic factor in hepatocellular carcinoma. *Hepatology*, **59**, 1900–1911.
23. Noubissi, F.K., Nikiforov, M.A., Colburn, N. and Spiegelman, V.S. (2010) Transcriptional Regulation of CRD-BP by c-myc: Implications for c-myc Functions. *Genes Cancer*, **1**, 1074–1082.
24. Degrauwe, N., Schlumpf, T.B., Janiszewska, M., Martin, P., Cauderay, A., Provero, P., Riggi, N., Suva, M.L., Paro, R. and Stamenkovic, I. (2016) The RNA binding protein IMP2 preserves glioblastoma stem cells by preventing let-7 target gene silencing. *Cell Rep.*, **15**, 1634–1647.
25. Degrauwe, N., Suva, M.L., Janiszewska, M., Riggi, N. and Stamenkovic, I. (2016) IMPs: an RNA-binding protein family that provides a link between stem cell maintenance in normal development and cancer. *Genes Dev.*, **30**, 2459–2474.
26. Nishino, J., Kim, S., Zhu, Y., Zhu, H. and Morrison, S.J. (2013) A network of heterochronic genes including Imp1 regulates temporal changes in stem cell properties. *Elife*, **2**, e00924.
27. JnBaptiste, C.K., Gurtan, A.M., Thai, K.K., Lu, V., Bhutkar, A., Su, M.J., Rotem, A., Jacks, T. and Sharp, P.A. (2017) Dicer loss and recovery induce an oncogenic switch driven by transcriptional activation of the oncofetal Imp1-3 family. *Genes Dev.*, **31**, 674–687.
28. Jonson, L., Christiansen, J., Hansen, T.V., Vikesa, J., Yamamoto, Y. and Nielsen, F.C. (2014) IMP3 RNP safe houses prevent miRNA-directed HMG2 mRNA decay in cancer and development. *Cell Rep.*, **7**, 539–551.
29. Kobel, M., Xu, H., Bourne, P.A., Spaulding, B.O., Shih, Ie, M., Mao, T.L., Soslow, R.A., Ewanowich, C.A., Kalloger, S.E., Mehl, E. *et al.* (2009) IGF2BP3 (IMP3) expression is a marker of unfavorable prognosis in ovarian carcinoma of clear cell subtype. *Mod. Pathol.*, **22**, 469–475.
30. Davidson, B., Rosenfeld, Y.B., Holth, A., Hellesylt, E., Trope, C.G., Reich, R. and Yisraeli, J.K. (2014) VICKZ2 protein expression in ovarian serous carcinoma effusions is associated with poor survival. *Hum. Pathol.*, **45**, 1520–1528.
31. Braun, J., Misiak, D., Busch, B., Krohn, K. and Huttelmaier, S. (2014) Rapid identification of regulatory microRNAs by miTRAP (miRNA trapping by RNA in vitro affinity purification). *Nucleic Acids Res.*, **42**, e66.
32. Kohn, M., Ihling, C., Sinz, A., Krohn, K. and Huttelmaier, S. (2015) The Y3** ncRNA promotes the 3' end processing of histone mRNAs. *Genes Dev.*, **29**, 1998–2003.
33. Kim, D., Perte, G., Trapnell, C., Pimentel, H., Kelley, R. and Salzberg, S.L. (2013) TopHat2: accurate alignment of transcriptomes in the presence of insertions, deletions and gene fusions. *Genome Biol.*, **14**, R36.
34. Langmead, B. and Salzberg, S.L. (2012) Fast gapped-read alignment with Bowtie 2. *Nat. Methods*, **9**, 357–359.
35. Liao, Y., Smyth, G.K. and Shi, W. (2014) featureCounts: an efficient general purpose program for assigning sequence reads to genomic features. *Bioinformatics*, **30**, 923–930.
36. Cunningham, F., Amode, M.R., Barrell, D., Beal, K., Billis, K., Brent, S., Carvalho-Silva, D., Clapham, P., Coates, G., Fitzgerald, S. *et al.* (2015) Ensembl 2015. *Nucleic Acids Res.*, **43**, D662–D669.
37. Kozomara, A. and Griffiths-Jones, S. (2014) miRBase: annotating high confidence microRNAs using deep sequencing data. *Nucleic Acids Res.*, **42**, D68–D73.
38. Robinson, M.D., McCarthy, D.J. and Smyth, G.K. (2010) edgeR: a Bioconductor package for differential expression analysis of digital gene expression data. *Bioinformatics*, **26**, 139–140.
39. Ru, Y., Kechris, K.J., Tabakoff, B., Hoffman, P., Radcliffe, R.A., Bowler, R., Mahaffey, S., Rossi, S., Calin, G.A., Bemis, L. *et al.* (2014) The multiMiR R package and database: integration of microRNA-target interactions along with their disease and drug associations. *Nucleic Acids Res.*, **42**, e133.
40. Hafner, M., Landthaler, M., Burger, L., Khorshid, M., Hausser, J., Berninger, P., Rothballer, A., Ascano, M. Jr, Jungkamp, A.C., Munschauer, M. *et al.* (2010) Transcriptome-wide identification of RNA-binding protein and microRNA target sites by PAR-CLIP. *Cell*, **141**, 129–141.
41. Van Nostrand, E.L., Pratt, G.A., Shishkin, A.A., Gelboin-Burkhart, C., Fang, M.Y., Sundararaman, B., Blue, S.M., Nguyen, T.B., Surka, C., Elkins, K. *et al.* (2016) Robust transcriptome-wide discovery of RNA-binding protein binding sites with enhanced CLIP (eCLIP). *Nat. Methods*, **13**, 508–514.
42. Conway, A.E., Van Nostrand, E.L., Pratt, G.A., Aigner, S., Wilbert, M.L., Sundararaman, B., Freese, P., Lambert, N.J., Sathe, S., Liang, T.Y. *et al.* (2016) Enhanced CLIP uncovers IMP Protein-RNA targets in human pluripotent stem cells important for cell adhesion and survival. *Cell Rep.*, **15**, 666–679.
43. Gottwein, E., Corcoran, D.L., Mukherjee, N., Skalsky, R.L., Hafner, M., Nusbaum, J.D., Shamulailatpam, P., Love, C.L., Dave, S.S., Tuschl, T. *et al.* (2011) Viral microRNA targetome of KSHV-infected primary effusion lymphoma cell lines. *Cell Host Microbe*, **10**, 515–526.
44. Kishore, S., Jaskiewicz, L., Burger, L., Hausser, J., Khorshid, M. and Zavolan, M. (2011) A quantitative analysis of CLIP methods for identifying binding sites of RNA-binding proteins. *Nat. Methods*, **8**, 559–564.
45. Skalsky, R.L., Corcoran, D.L., Gottwein, E., Frank, C.L., Kang, D., Hafner, M., Nusbaum, J.D., Feederle, R., Delecluse, H.J., Luftig, M.A. *et al.* (2012) The viral and cellular microRNA targetome in lymphoblastoid cell lines. *PLoS Pathog.*, **8**, e1002484.
46. Subramanian, A., Tamayo, P., Mootha, V.K., Mukherjee, S., Ebert, B.L., Gillette, M.A., Paulovich, A., Pomeroy, S.L., Golub, T.R., Lander, E.S. *et al.* (2005) Gene set enrichment analysis: a knowledge-based approach for interpreting genome-wide expression profiles. *Proc. Natl. Acad. Sci. U.S.A.*, **102**, 15545–15550.
47. Wurth, L., Papasaikas, P., Olmeda, D., Bley, N., Calvo, G.T., Guerrero, S., Cerezo-Wallis, D., Martinez-Useros, J., Garcia-Fernandez, M., Huttelmaier, S. *et al.* (2016) UNR/CSDE1 drives a post-transcriptional program to promote melanoma invasion and metastasis. *Cancer Cell*, **30**, 694–707.
48. Lanczky, A., Nagy, A., Bottai, G., Munkacsy, G., Szabo, A., Santarpia, L. and Györfy, B. (2016) miRpower: a web-tool to validate survival-associated miRNAs utilizing expression data from 2178 breast cancer patients. *Breast Cancer Res. Treat.*, **160**, 439–446.
49. Domcke, S., Sinha, R., Levine, D.A., Sander, C. and Schultz, N. (2013) Evaluating cell lines as tumour models by comparison of genomic profiles. *Nat. Commun.*, **4**, 2126.
50. Wachter, K., Kohn, M., Stohr, N. and Huttelmaier, S. (2013) Subcellular localization and RNP formation of IGF2BPs (IGF2 mRNA-binding proteins) is modulated by distinct RNA-binding domains. *Biol. Chem.*, **394**, 1077–1090.
51. Zhao, W., Lu, D., Liu, L., Cai, J., Zhou, Y., Yang, Y., Zhang, Y. and Zhang, J. (2017) Insulin-like growth factor 2 mRNA binding protein 3 (IGF2BP3) promotes lung tumorigenesis via attenuating p53 stability. *Oncotarget*, **8**, 93672–93687.

52. Zirkel,A., Lederer,M., Stohr,N., Pazaitis,N. and Huttelmaier,S. (2013) IGF2BP1 promotes mesenchymal cell properties and migration of tumor-derived cells by enhancing the expression of LEF1 and SNAI2 (SLUG). *Nucleic Acids Res.*, **41**, 6618–6636.
53. Mongroo,P.S., Noubissi,F.K., Cuatrecasas,M., Kalabis,J., King,C.E., Johnstone,C.N., Bowser,M.J., Castells,A., Spiegelman,V.S. and Rustgi,A.K. (2011) IMP-1 displays cross-talk with K-Ras and modulates colon cancer cell survival through the novel proapoptotic protein CYFIP2. *Cancer Res.*, **71**, 2172–2182.
54. Hart,T., Chandrashekar,M., Aregger,M., Steinhart,Z., Brown,K.R., MacLeod,G., Mis,M., Zimmermann,M., Fradet-Turcotte,A., Sun,S. *et al.* (2015) High-resolution CRISPR screens reveal fitness genes and genotype-specific cancer liabilities. *Cell*, **163**, 1515–1526.
55. Elcheva,I., Tarapore,R.S., Bhatia,N. and Spiegelman,V.S. (2008) Overexpression of mRNA-binding protein CRD-BP in malignant melanomas. *Oncogene*, **27**, 5069–5074.
56. Elkhadragy,L., Chen,M., Miller,K., Yang,M.H. and Long,W. (2017) A regulatory BMI1/let-7i/ERK3 pathway controls the motility of head and neck cancer cells. *Mol. Oncol.*, **11**, 194–207.
57. Xu,D., Takeshita,F., Hino,Y., Fukunaga,S., Kudo,Y., Tamaki,A., Matsunaga,J., Takahashi,R.U., Takata,T., Shimamoto,A. *et al.* (2011) miR-22 represses cancer progression by inducing cellular senescence. *J. Cell Biol.*, **193**, 409–424.
58. Dai,N., Ji,F., Wright,J., Minichiello,L., Sadreyev,R. and Avruch,J. (2017) IGF2 mRNA binding protein-2 is a tumor promoter that drives cancer proliferation through its client mRNAs IGF2 and HMGA1. *Elife*, **6**, e27155.
59. Huttelmaier,S., Zenklusen,D., Lederer,M., Dichtenberg,J., Lorenz,M., Meng,X., Bassell,G.J., Condeelis,J. and Singer,R.H. (2005) Spatial regulation of beta-actin translation by Src-dependent phosphorylation of ZBP1. *Nature*, **438**, 512–515.
60. Elcheva,I., Goswami,S., Noubissi,F.K. and Spiegelman,V.S. (2009) CRD-BP protects the coding region of betaTrCP1 mRNA from miR-183-mediated degradation. *Mol. Cell*, **35**, 240–246.
61. Hammerle,M., Gutschner,T., Uckelmann,H., Ozgur,S., Fiskin,E., Gross,M., Skawran,B., Geffers,R., Longerich,T., Breuhahn,K. *et al.* (2013) Posttranscriptional destabilization of the liver-specific long noncoding RNA HULC by the IGF2 mRNA-binding protein 1 (IGF2BP1). *Hepatology*, **58**, 1703–1712.
62. Li,Y., Estep,J.A. and Karginov,F.V. (2018) Transcriptome-wide identification and validation of interactions between the miRNA machinery and HuR on mRNA targets. *J. Mol. Biol.*, **430**, 285–296.